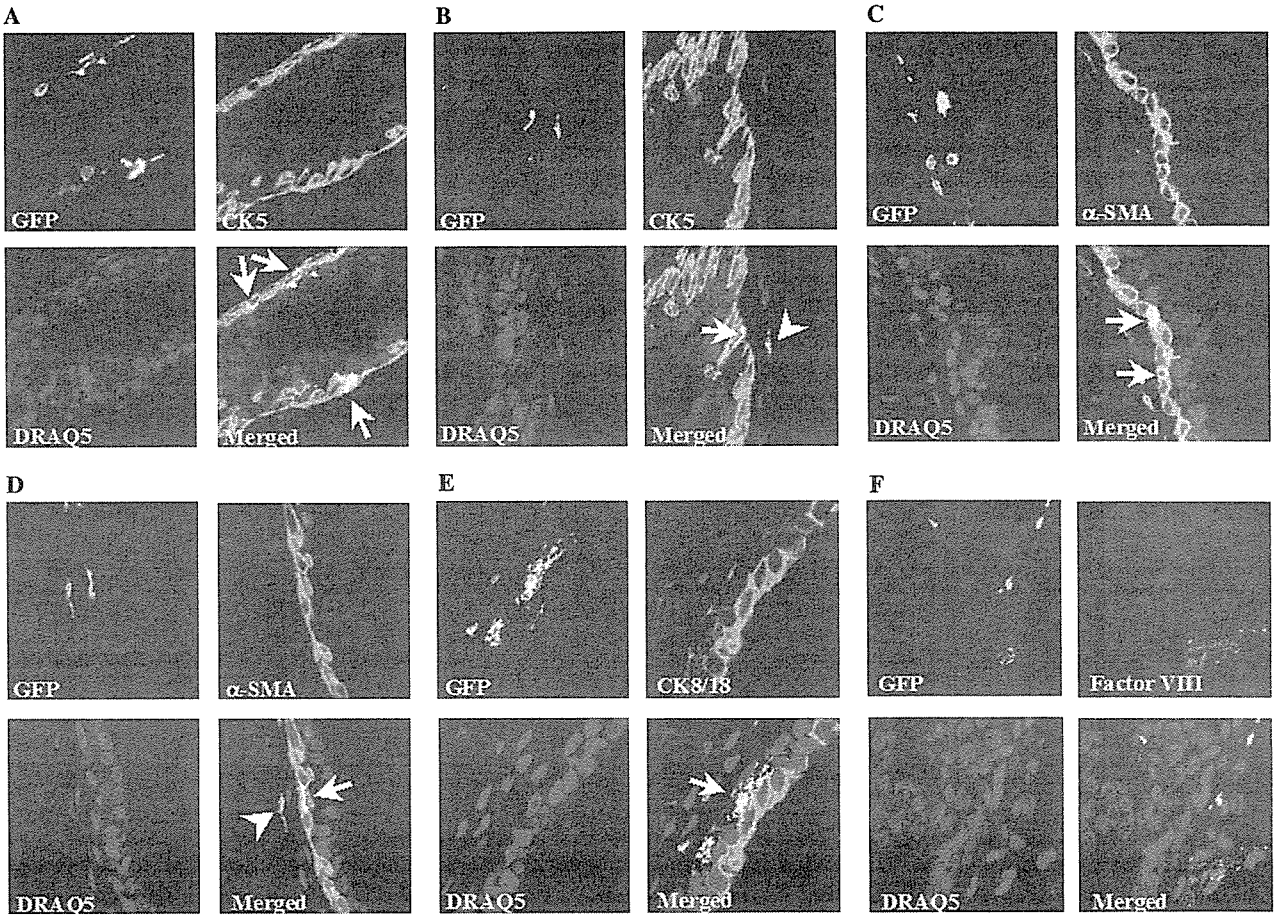

Fig. 2. Immunofluorescent staining for CK5, α-SMA (marker for myoepithelial cells), CK8/18 (for luminal epithelial cells), Factor VIII (for endothelial cells), and GFP in $BMT^{GFP+/-}$ mice. The slides were counterstained with DRAQ5 for the discrimination of nucleated cells. (A,B) Fluorescent image of mammary gland stained for GFP and CK5. Cytokeratin 5 is expressed in outer layer of the ductal epithelial cells. Arrows indicate GFP and CK5 double positive epithelial cells (BM-derived myoepithelial cells). Arrowhead indicates GFP-positive fibroblast (BM-derived periductal fibroblast) that located just outside of the CK5-positive layer. (C,D) Fluorescent image of GFP and α-SMA. The basal layer of the ductal epithelial cells expresses α-SMA. Arrows indicate GFP and α-SMA double positive epithelial cells (BM-derived myoepithelial cells). GFP-positive fibroblast (BM-derived periductal fibroblast, arrowhead) is located just outside of duct. (E) Fluorescent image of GFP and CK8/18. The luminal epithelial layer is CK8/18 positive. Arrow indicates GFP-positive cell that located in ductal basal layer does not coexpress CK8/18. (F) Fluorescent image of GFP and Factor VIII. Factor VIII positive cells do not coexpress GFP.

results indicate that BM can be a source of both myoepithelial cells and periductal fibroblasts in BMT mice.

To confirm the recruitment of myoepithelial cells and periductal fibroblasts without irradiation, whole mammary fat pad containing both epithelium and stroma was removed from 3 week-old GFP−/− mice and was transplanted into the abdominal wall of GFP Tg mice (Fig. 3A). At 10 weeks of age, transplanted mammary gland from GFP−/− mice into GFP Tg mice was analyzed. When WMT was performed from GFP−/− mice to GFP−/− mice, no GFP-positive cells were detected (Fig. 3B). On the contrary, certain myoepithelial cells and periductal fibroblasts in the mammary gland transplanted from GFP−/− mice to GFP Tg mice were GFP positive (Fig. 3C and D). The numbers of GFP-positive myoepithelial cells in mammary gland of BMT mice and WMT mice were 7.6 ± 2.0 and 6.0 ± 0.9, respectively ($P = 0.4971$, Fig. 3E). The numbers of periductal fibroblasts in BMT mice and WMT mice were 13.2 ± 1.2 and 13.0 ± 2.8, respectively ($P = 0.9492$, Fig. 3F). There were no significant differences in the numbers of BM-derived myoepithelial cells and periductal fibroblasts between BMT and WMT mice.

BM-derived myoepithelial cells and periductal fibroblasts are recruited into mammary glands during pubertal and postpubertal stages

We examined whether engraftment of BM-derived myoepithelial cells and periductal fibroblasts occurs even in the postpubertal stage. At 10 weeks of age, mice were transplanted with GFP Tg BM cells, and mammary glands were analyzed after 7 weeks. The numbers of myoepithelial cells and periductal fibroblasts in BMT^{3w} mice at 10 week old were 7.6 ± 2.0 and 13.2 ± 1.2, respectively. Otherwise, the numbers of myoepithelial cells and periductal fibroblasts in BMT^{10w} mice were 1.6 ± 0.2 and 5.4 ± 1.1, respectively, and showed significant decreases as compared with those of BMT^{3w} mice (Fig. 4A and B).

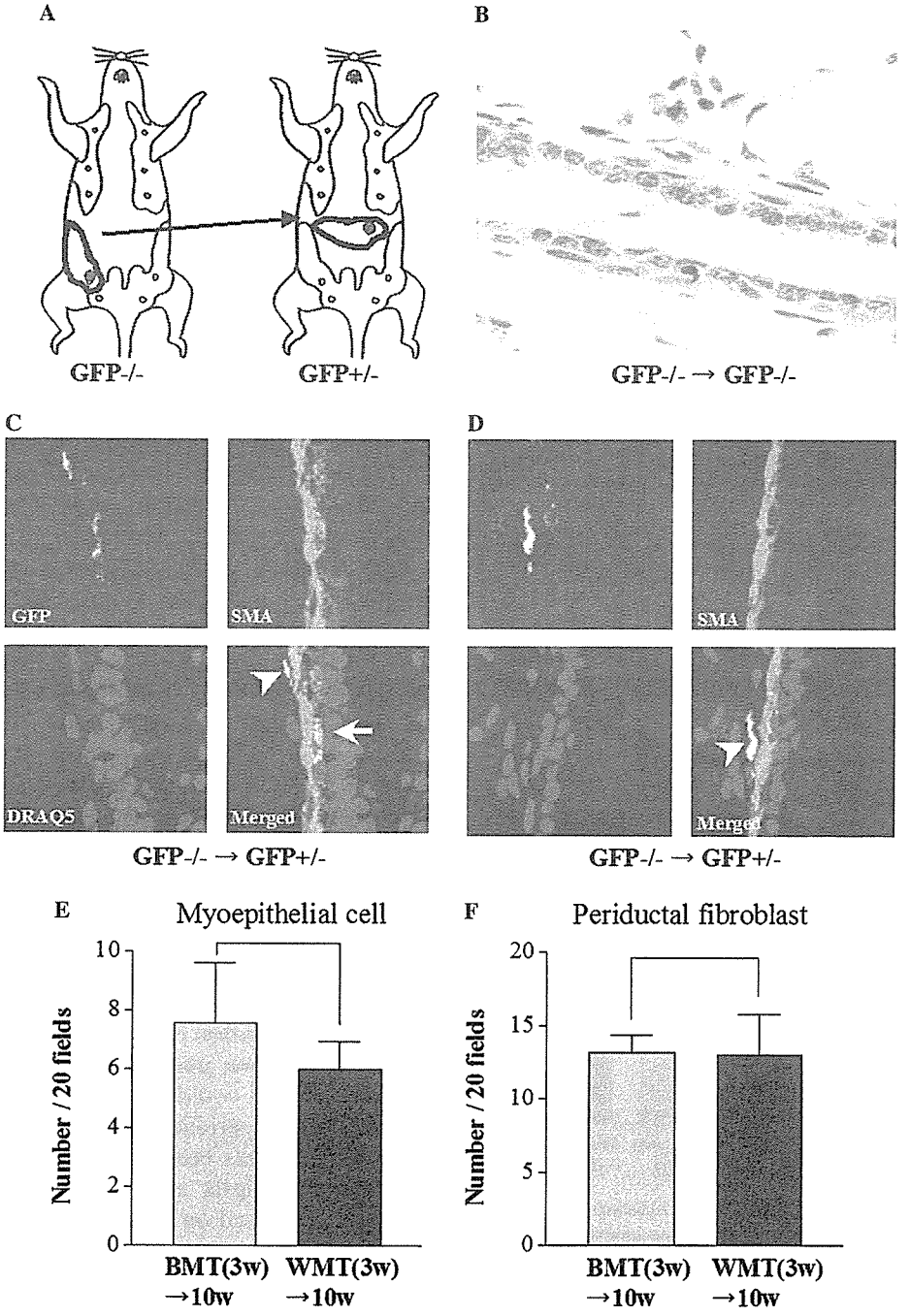

Fig. 3. (A) Schematic representation of WMT. The entire fourth mammary glands of 3 week-old GFP−/− mice were transplanted into the abdominal walls of 3 week-old GFP Tg mice. At 10 weeks of age, GFP−/− mammary glands transplanted into GFP Tg mice were analyzed. (B) Immunohistochemical staining for GFP of WMT control mice. There were no GFP-positive cells in GFP−/− mammary glands transplanted into GFP−/− mice. (C,D) Fluorescent image of GFP and α-SMA of WMT mice. Arrows indicate GPF and α-SMA double positive epithelial cells (BM-derived myoepithelial cells). GFP-positive fibroblast (BM-derived periductal fibroblast, arrowhead) is located just outside of duct. (E,F) The numbers of GFP-positive myoepithelial cells (E) and periductal fibroblasts (F) recruited into mammary gland of BMT mice and WMT mice during pubertal stages. Data represent means ± SE for each five mice.

Treatment with estrogen + progesterone increased recruitment of BM-derived myoepithelial cells and periductal fibroblasts

Mammary glands change the structure dramatically during postnatal development and pregnancy, and estradiol and progesterone are required for the remodeling of mammary grand in adult mice [32,36]. An estrogen + progesterone pellet was implanted into the subcutaneous tissues of BMT^{10w} mice at 14 weeks and mammary glands were harvested and analyzed after 21 days. Whole mount preparations stained with carmine red revealed that ductal

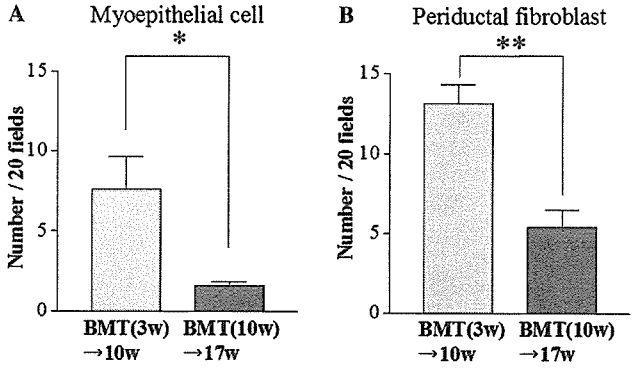

Fig. 4. The numbers of BM-derived myoepithelial cells (A) and periductal fibroblasts (B) recruited into mammary glands of BMT mice during pubertal and postpubertal stages. Three and 10 week-old mice were transplanted with GFP Tg BM cells, and mammary glands were analyzed after 7 weeks. Data represent means ± SE for each five mice. $*P = 0.0193$, $**P = 0.0011$.

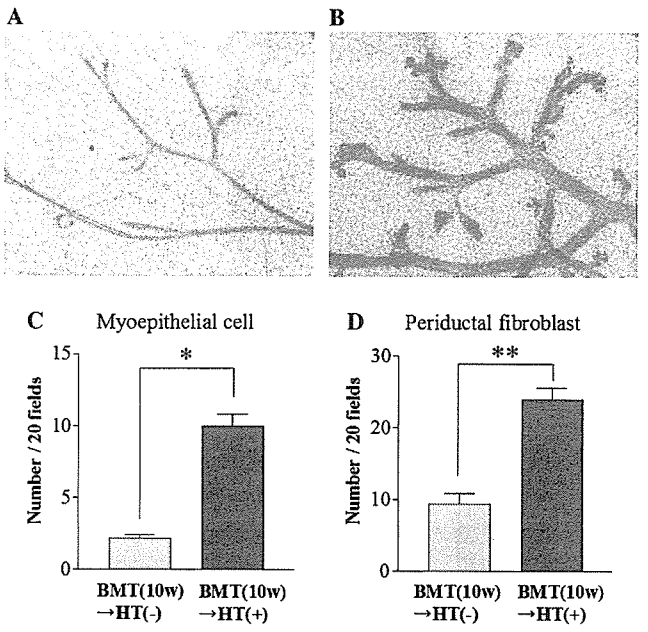

Fig. 5. Treatment of BMT mice with estrogen + progesterone increased recruitment of BM-derived myoepithelial cells and periductal fibroblasts into mammary gland. (A,B) Mammary gland whole mount preparations of hormone treated (HT) mice (B) and placebo mice (A) were stained with carmine red. (C,D) The numbers of GFP-positive myoepithelial cells (C) and periductal fibroblasts (D) recruited into mammary glands of BMT mice with or without estrogen + progesterone. Data represent means ± SE for each five mice. $*P = 0.0002$, $**P < 0.0001$.

dilation and side branching were prominent in mammary glands of hormone treated (HT) mice (Fig. 5B) as compared to placebo mice (Fig. 5A). The numbers of GFP-positive myoepithelial cells and periductal fibroblasts in placebo mice were 2.2 ± 0.2 and 9.4 ± 1.5, respectively. The numbers of GFP-positive myoepithelial cells and periductal fibroblasts in HT mice were significantly increased in placebo mice (10.0 ± 0.8 and 24.0 ± 1.6, respectively, Fig. 5C and D).

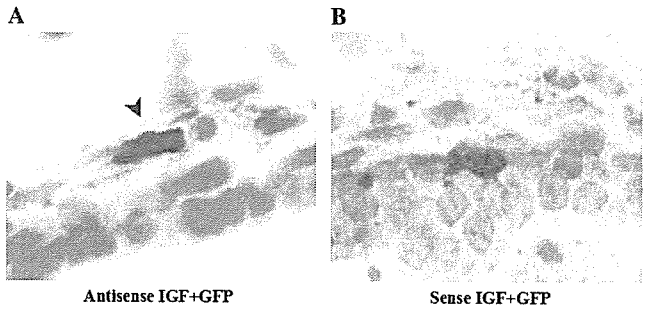

Fig. 6. *In situ* hybridization for IGF-I mRNA and GFP immunostaining. (A) *In situ* hybridization for antisense IGF-I probe. Arrowhead indicates a GFP-positive periductal fibroblast, which also shows the signal for IGF-I mRNAs. (B) *In situ* hybridization for sense IGF-I probe. No IGF-I mRNAs-positive cells can be seen.

IGF-I mRNA expression in periductal fibroblasts

IGF-I reportedly acts in several physiological states of the mammary gland. We performed *in situ* hybridization for IGF-I mRNAs followed by GFP immunostaining. IGF-I mRNAs were expressed uniformly along the ducts but they were of undetectable level within both myoepithelial and luminal epithelial cells. Furthermore, IGF-I mRNAs were detected in GFP-positive periductal fibroblasts (Fig. 6A, arrowhead). No IGF-I mRNAs were detected in the specimen treated with sense IGF-I probe (Fig. 6B).

Discussion

Recent investigations have found that BM-derived cells are a constituent of normal organs, and that these cells are efficiently recruited in the context of remodeling tissue such as cancer, granulation tissue, and fibrosis [27–29,37]. In the current study, we used BMT mice model and clearly showed that BM could serve progenitor cells for myoepithelial cells and periductal fibroblasts of the mouse mammary gland. It has been reported that mesenchymal cells including fibroblasts are important in mammary gland development, based on their interactions with the epithelium [38–41], and that myoepithelial cells play essential roles in physiological establishment of the mammary epithelial bilayer and in pathological development [42–45]. The findings that BM-derived periductal fibroblasts and myoepithelial cells were engrafted into the mammary gland during not only the pubertal but also the postpubertal stage and that hormonal stimulation significantly increased the engraftment of these cells suggest the functional importance of such cells in the regulation of mammary gland development as well as physiological homeostasis.

The current observation that BM-derived periductal fibroblasts expressed IGF-I mRNAs in mouse mammary glands also supports this idea. IGF-I has a role in postnatal development of the mammary gland and is a potent mitogen for normal and tumorigenic mammary epithelial cells [46]. A previous report indicated that IGF-I mRNA was expressed mainly in periductal stromal tissue [47]. IGF-I

also stimulates mammary ductal growth by synergizing with and enhancing estrogen and progesterone actions [36,48]. Since periductal fibroblasts reside immediately adjacent to the basement membrane of mammary gland epithelial cells, IGF-I secreted from periductal fibroblasts may increase epithelial cell responsiveness to estrogen and influence epithelial cell growth, and ultimately determine epithelial cell fate. Taken together, our results support the emerging paradigm that BM-derived cells function as playing direct or indirect roles in mammary epithelial cell growth, rather than providing a source of "building blocks" for mammary gland morphogenesis.

BM contained progenitors for myoepithelial cell but not for ductal epithelial cell. The reason for this phenomenon remains unclear, however, it would be plausible that spatial distribution of the different functional units from different cellular lineages is strictly regulated. And this might be essential for the homeostasis of ductal structure of mammary gland. Although the possibility of cell fusion is incontrovertible, a recent report showed BM-derived epithelial cells, myofibroblasts, and fibroblasts in some remodeling tissue arise via a mechanism other than cell fusion [49–51].

As irradiation causes irreversible long-standing biological changes in the mammary stroma [52–54], it must be kept in mind that BMT model may be influenced by irradiation damage. We performed whole mammary gland transplantation, the process of which does not include irradiation. The results again demonstrated almost equal numbers of myoepithelial cells and periductal fibroblasts to be GFP positive. Little angiogenesis, granulation, and fibrosis were observed in surroundings of the transplanted fat pad in this model. Although BM-derived cells contribute to vasculogenesis and fibrosis after inflammation [22,23,26,27,55], it seems that healing the WMT wound had little influence on contribution of BM-derived cells to the mammary gland inside the transplanted fat pad. Therefore, we speculated that the contribution of BM cells to myoepithelial cells and periductal fibroblasts in mammary gland would be an actual physiological event.

In this study, we found that BM-derived cells could serve as the progenitors of mouse mammary gland component, myoepithelial cells, and periductal fibroblasts. Much work on the biological mechanisms underlying the recruitment of these cells is needed and this would provide important insights into the functional interplay between mammary gland epithelium and BM-derived cells.

Acknowledgments

We thank Chie Okumura and Yoko Okuhara for their expert technical assistance, and Motoko Suzaki for secretarial assistance.

References

[1] L. Hennighausen, G.W. Robinson, Signaling pathways in mammary gland development, Dev. Cell 1 (2001) 467–475.

[2] B.S. Wiseman, Z. Werb, Stromal effects on mammary gland development and breast cancer, Science 296 (2002) 1046–1049.

[3] M.A. Deugnier, E.P. Moiseyeva, J.P. Thiery, M. Glukhova, Myoepithelial cell differentiation in the developing mammary gland: progressive acquisition of smooth muscle phenotype, Dev. Dyn. 204 (1995) 107–117.

[4] J.M. Williams, C.W. Daniel, Mammary ductal elongation: differentiation of myoepithelium and basal lamina during branching morphogenesis, Dev. Biol. 97 (1983) 274–290.

[5] E.J. Ormerod, P.S. Rudland, Cellular composition and organization of ductal buds in developing rat mammary glands: evidence for morphological intermediates between epithelial and myoepithelial cells, Am. J. Anat. 170 (1984) 631–652.

[6] A. Sapino, L. Macri, P. Gugliotta, D. Pacchioni, Y.J. Liu, D. Medina, G. Bussolati, Immunophenotypic properties and estrogen dependency of budding cell structures in the developing mouse mammary gland, Differentiation 55 (1993) 13–18.

[7] A. Plath-Gabler, C. Gabler, F. Sinowatz, B. Berisha, D. Schams, The expression of the IGF family and GH receptor in the bovine mammary gland, J. Endocrinol. 168 (2001) 39–48.

[8] S.F. Wojcik, C.C. Capen, T.J. Rosol, Expression of PTHrP and the PTH/PTHrP receptor in purified alveolar epithelial cells, myoepithelial cells, and stromal fibroblasts derived from the lactating rat mammary gland, Exp. Cell Res. 248 (1999) 415–422.

[9] E.E. Herrington, T.G. Ram, D.S. Salomon, G.R. Johnson, W.J. Gullick, N. Kenney, H.L. Hosick, Expression of epidermal growth factor-related proteins in the aged adult mouse mammary gland and their relationship to tumorigenesis, J. Cell Physiol. 170 (1997) 47–56.

[10] L.R. Lund, J. Romer, N. Thomasset, H. Solberg, C. Pyke, M.J. Bissell, K. Dano, Z. Werb, Two distinct phases of apoptosis in mammary gland involution: proteinase-independent and -dependent pathways, Development 122 (1996) 181–193.

[11] J.J. Gomm, J. Smith, G.K. Ryall, R. Baillie, L. Turnbull, R.C. Coombes, Localization of basic fibroblast growth factor and transforming growth factor beta 1 in the human mammary gland, Cancer Res. 51 (1991) 4685–4692.

[12] V. Gouon-Evans, M.E. Rothenberg, J.W. Pollard, Postnatal mammary gland development requires macrophages and eosinophils, Development 127 (2000) 2269–2282.

[13] G. Ferrari, G. Cusella-De Angelis, M. Coletta, E. Paolucci, A. Stornaiuolo, G. Cossu, F. Mavilio, Muscle regeneration by bone marrow-derived myogenic progenitors, Science 279 (1998) 1528–1530.

[14] K. Shimizu, S. Sugiyama, M. Aikawa, Y. Fukumoto, E. Rabkin, P. Libby, R.N. Mitchell, Host bone-marrow cells are a source of donor intimal smooth-muscle-like cells in murine aortic transplant arteriopathy, Nat. Med. 7 (2001) 738–741.

[15] S.Y. Corbel, A. Lee, L. Yi, J. Duenas, T.R. Brazelton, H.M. Blau, F.M. Rossi, Contribution of hematopoietic stem cells to skeletal muscle, Nat. Med. 9 (2003) 1528–1532.

[16] S. Makino, K. Fukuda, S. Miyoshi, F. Konishi, H. Kodama, J. Pan, M. Sano, T. Takahashi, S. Hori, H. Abe, J. Hata, A. Umezawa, S. Ogawa, Cardiomyocytes can be generated from marrow stromal cells in vitro, J. Clin. Invest. 103 (1999) 697–705.

[17] K.A. Jackson, S.M. Majka, H. Wang, J. Pocius, C.J. Hartley, M.W. Majesky, M.L. Entman, L.H. Michael, K.K. Hirschi, M.A. Goodell, Regeneration of ischemic cardiac muscle and vascular endothelium by adult stem cells, J. Clin. Invest. 107 (2001) 1395–1402.

[18] D. Orlic, J. Kajstura, S. Chimenti, I. Jakoniuk, S.M. Anderson, B. Li, J. Pickel, R. McKay, B. Nadal-Ginard, D.M. Bodine, A. Leri, P. Anversa, Bone marrow cells regenerate infarcted myocardium, Nature 410 (2001) 701–705.

[19] B.E. Petersen, W.C. Bowen, K.D. Patrene, W.M. Mars, A.K. Sullivan, N. Murase, S.S. Boggs, J.S. Greenberger, J.P. Goff, Bone marrow as a potential source of hepatic oval cells, Science 284 (1999) 1168–1170.

[20] M.R. Alison, R. Poulsom, R. Jeffery, A.P. Dhillon, A. Quaglia, J. Jacob, M. Novelli, G. Prentice, J. Williamson, N.A. Wright, Hepatocytes from non-hepatic adult stem cells, Nature 406 (2000) 257.

[21] E. Lagasse, H. Connors, M. Al-Dhalimy, M. Reitsma, M. Dohse, L. Osborne, X. Wang, M. Finegold, I.L. Weissman, M. Grompe, Purified hematopoietic stem cells can differentiate into hepatocytes in vivo, Nat. Med. 6 (2000) 1229–1234.
[22] T. Asahara, H. Masuda, T. Takahashi, C. Kalka, C. Pastore, M. Silver, M. Kearne, M. Magner, J.M. Isner, Bone marrow origin of endothelial progenitor cells responsible for postnatal vasculogenesis in physiological and pathological neovascularization, Circ. Res. 85 (1999) 221–228.
[23] M. Sata, A. Saiura, A. Kunisato, A. Tojo, S. Okada, T. Tokuhisa, H. Hirai, M. Makuuchi, Y. Hirata, R. Nagai, Hematopoietic stem cells differentiate into vascular cells that participate in the pathogenesis of atherosclerosis, Nat. Med. 8 (2002) 403–409.
[24] M. Iwano, D. Plieth, T.M. Danoff, C. Xue, H. Okada, E.G. Neilson, Evidence that fibroblasts derive from epithelium during tissue fibrosis, J. Clin. Invest. 110 (2002) 341–350.
[25] N. Hashimoto, H. Jin, T. Liu, S.W. Chensue, S.H. Phan, Bone marrow-derived progenitor cells in pulmonary fibrosis, J. Clin. Invest. 113 (2004) 243–252.
[26] M. Brittan, T. Hunt, R. Jeffery, R. Poulsom, S.J. Forbes, K. Hodivala-Dilke, J. Goldman, M.R. Alison, N.A. Wright, Bone marrow derivation of pericryptal myofibroblasts in the mouse and human small intestine and colon, Gut 50 (2002) 752–757.
[27] N.C. Direkze, S.J. Forbes, M. Brittan, T. Hunt, R. Jeffery, S.L. Preston, R. Poulsom, K. Hodivala-Dilke, M.R. Alison, N.A. Wright, Multiple organ engraftment by bone-marrow-derived myofibroblasts and fibroblasts in bone-marrow-transplanted mice, Stem Cells 21 (2003) 514–520.
[28] G. Ishii, T. Sangai, T. Oda, Y. Aoyagi, T. Hasebe, N. Kanomata, Y. Endoh, C. Okumura, Y. Okuhara, J. Magae, M. Emura, T. Ochiya, A. Ochiai, Bone-marrow-derived myofibroblasts contribute to the cancer-induced stromal reaction, Biochem. Biophys. Res. Commun. 309 (2003) 232–240.
[29] T. Sangai, G. Ishii, K. Kodama, S. Miyamoto, Y. Aoyagi, T. Ito, J. Magae, H. Sasaki, T. Nagashima, M. Miyazaki, A. Ochiai, Effect of differences in cancer cells and tumor growth sites on recruiting bone marrow-derived endothelial cells and myofibroblasts in cancer-induced stroma, Int. J. Cancer 115 (2005) 885–892.
[30] M. Okabe, M. Ikawa, K. Kominami, T. Nakanishi, Y. Nishimune, 'Green mice' as a source of ubiquitous green cells, FEBS Lett. 407 (1997) 313–319.
[31] C. Brisken, S. Park, T. Vass, J.P. Lydon, B.W. O'Malley, R.A. Weinberg, A paracrine role for the epithelial progesterone receptor in mammary gland development, Proc. Natl. Acad. Sci. USA 95 (1998) 5076–5081.
[32] W.P. Bocchinfuso, J.K. Lindzey, S.C. Hewitt, J.A. Clark, P.H. Myers, R. Cooper, K.S. Korach, Induction of mammary gland development in estrogen receptor-alpha knockout mice, Endocrinology 141 (2000) 2982–2994.
[33] S. Kitazawa, R. Kitazawa, RANK ligand is a prerequisite for cancer-associated osteolytic lesions, J. Pathol. 198 (2002) 228–236.
[34] L. Ronnov-Jessen, O.W. Petersen, M.J. Bissell, Cellular changes involved in conversion of normal to malignant breast: importance of the stromal reaction, Physiol. Rev. 76 (1996) 69–125.
[35] W. Bocker, R. Moll, C. Poremba, R. Holland, P.J. Van Diest, P. Dervan, H. Burger, D. Wai, R. Ina Diallo, B. Brandt, H. Herbst, A. Schmidt, M.M. Lerch, I.B. Buchwallow, Common adult stem cells in the human breast give rise to glandular and myoepithelial cell lineages: a new cell biological concept, Lab. Invest. 82 (2002) 737–746.
[36] W. Ruan, M.E. Monaco, D.L. Kleinberg, Progesterone stimulates mammary gland ductal morphogenesis by synergizing with and enhancing insulin-like growth factor-I action, Endocrinology 146 (2005) 1170–1178.
[37] G. Ishii, T. Sangai, K. Sugiyama, T. Ito, T. Hasebe, Y. Endoh, J. Magae, A. Ochiai, In vivo characterization of bone marrow-derived fibroblasts recruited into fibrotic lesions, Stem Cells 23 (2005) 699–706.
[38] Y. Yang, E. Spitzer, D. Meyer, M. Sachs, C. Niemann, G. Hartmann, K.M. Weidner, C. Birchmeier, W. Birchmeier, Sequential requirement of hepatocyte growth factor and neuregulin in the morphogenesis and differentiation of the mammary gland, J. Cell Biol. 131 (1995) 215–226.
[39] M. Sasaki, J. Enami, Mammary fibroblast-derived hepatocyte growth factor and mammogenic hormones stimulate the growth of mouse mammary epithelial cells in primary culture, Endocr. J. 46 (1999) 359–366.
[40] K.M. Darcy, D. Zangani, W. Shea-Eaton, S.F. Shoemaker, P.P. Lee, L.H. Mead, A. Mudipalli, R. Megan, M.M. Ip, Mammary fibroblasts stimulate growth, alveolar morphogenesis, and functional differentiation of normal rat mammary epithelial cells, In Vitro Cell Dev. Biol. Anim. 36 (2000) 578–592.
[41] H.Z. Zhang, J.M. Bennett, K.T. Smith, N. Sunil, S.Z. Haslam, Estrogen mediates mammary epithelial cell proliferation in serum-free culture indirectly via mammary stroma-derived hepatocyte growth factor, Endocrinology 143 (2002) 3427–3434.
[42] Z. Nikolova, V. Djonov, G. Zuercher, A.C. Andres, A. Ziemiecki, Cell-type specific and estrogen dependent expression of the receptor tyrosine kinase EphB4 and its ligand ephrin-B2 during mammary gland morphogenesis, J. Cell Sci. 111 (Pt 18) (1998) 2741–2751.
[43] M.A. Deugnier, J. Teuliere, M.M. Faraldo, J.P. Thiery, M.A. Glukhova, The importance of being a myoepithelial cell, Breast Cancer Res. 4 (2002) 224–230.
[44] P.M. Ismail, F.J. DeMayo, P. Amato, J.P. Lydon, Progesterone induction of calcitonin expression in the murine mammary gland, J. Endocrinol. 180 (2004) 287–295.
[45] J. Teuliere, M.M. Faraldo, M.A. Deugnier, M. Shtutman, A. Ben-Ze'ev, J.P. Thiery, M.A. Glukhova, Targeted activation of beta-catenin signaling in basal mammary epithelial cells affects mammary development and leads to hyperplasia, Development 132 (2005) 267–277.
[46] E. Marshman, C.H. Streuli, Insulin-like growth factors and insulin-like growth factor binding proteins in mammary gland function, Breast Cancer Res. 4 (2002) 231–239.
[47] M.M. Richert, T.L. Wood, The insulin-like growth factors (IGF) and IGF type I receptor during postnatal growth of the murine mammary gland: sites of messenger ribonucleic acid expression and potential functions, Endocrinology 140 (1999) 454–461.
[48] W. Ruan, V. Catanese, R. Wieczorek, M. Feldman, D.L. Kleinberg, Estradiol enhances the stimulatory effect of insulin-like growth factor-I (IGF-I) on mammary development and growth hormone-induced IGF-I messenger ribonucleic acid, Endocrinology 136 (1995) 1296–1302.
[49] N.C. Direkze, K. Hodivala-Dilke, R. Jeffery, T. Hunt, R. Poulsom, D. Oukrif, M.R. Alison, N.A. Wright, Bone marrow contribution to tumor-associated myofibroblasts and fibroblasts, Cancer Res. 64 (2004) 8492–8495.
[50] T.C. Fang, M.R. Alison, H.T. Cook, R. Jeffery, N.A. Wright, R. Poulsom, Proliferation of bone marrow-derived cells contributes to regeneration after folic acid-induced acute tubular injury, J. Am. Soc. Nephrol. 16 (2005) 1723–1732.
[51] T. Matsumoto, R. Okamoto, T. Yajima, T. Mori, S. Okamoto, Y. Ikeda, M. Mukai, M. Yamazaki, S. Oshima, K. Tsuchiya, T. Nakamura, T. Kanai, H. Okano, J. Inazawa, T. Hibi, M. Watanabe, Increase of bone marrow-derived secretory lineage epithelial cells during regeneration in the human intestine, Gastroenterology 128 (2005) 1851–1867.
[52] R.F. Hagemann, C.P. Sigdestad, S. Lesher, Intestinal crypt survival and total and per crypt levels of proliferative cellularity following irradiation: single X-ray exposures, Radiat. Res. 46 (1971) 533–546.
[53] T. Amano, T. Inamura, C.M. Wu, S. Kura, A. Nakamizo, S. Inoha, M. Miyazono, K. Ikezaki, Effects of single low dose irradiation on subventricular zone cells in juvenile rat brain, Neurol. Res. 24 (2002) 809–816.
[54] M.H. Barcellos-Hoff, Integrative radiation carcinogenesis: interactions between cell and tissue responses to DNA damage, Semin. Cancer Biol. 15 (2005) 138–148.
[55] M. Brittan, V. Chance, G. Elia, R. Poulsom, M.R. Alison, T.T. MacDonald, N.A. Wright, A regenerative role for bone marrow following experimental colitis: contribution to neovasculogenesis and myofibroblasts, Gastroenterology 128 (2005) 1984–1995.

Available online at www.sciencedirect.com
SCIENCE DIRECT
Cellular Signalling 18 (2006) 994–1005
CELLULAR SIGNALLING
www.elsevier.com/locate/cellsig

ERK is an anti-inflammatory signal that suppresses expression of NF-κB-dependent inflammatory genes by inhibiting IKK activity in endothelial cells

Yong-Sun Maeng [a,1], Jeong-Ki Min [a,1], Jeong Hun Kim [b], Akiko Yamagishi [c], Naoki Mochizuki [c], Ja-Young Kwon [d], Yong-Won Park [d], Young-Myeong Kim [e], Young-Guen Kwon [a,*]

[a] *Department of Biochemistry College of Sciences, Yonsei University, Seoul 120-749, Korea*
[b] *Department of Ophthalmology Seoul National University College of Medicine, Seoul Artificial Eye Center, Clinical Research Institute, Seoul National University Hospital, Seoul 110-744, Korea*
[c] *Department of Structural Analysis, National Cardiovascular Center Research Institute, 5-7-1 Fujishirodai, Suita, Osaka 565-8565, Japan*
[d] *Department of Obstetrics and Gynecology Yonsei University College of Medicine 134 Shinchon-dong, Seodaemoon-gu Seoul 120-752, Korea*
[e] *Department of Molecular and Cellular Biochemistry, School of Medicine, Kangwon National University, Chunchon, Kangwon-Do 200-701, Korea*

Received 29 July 2005; received in revised form 20 August 2005; accepted 22 August 2005
Available online 20 October 2005

Abstract

Unveiling of endothelial nuclear factor-κB (NF-κB) activation is pivotal for understanding the inflammatory reaction and the pathogenesis of inflammatory vascular diseases. We here report the novel function of extracellular signal-related kinase (ERK) in controlling endothelial NF-κB activation and inflammatory responses. In human endothelial cells, vascular endothelial growth factor (VEGF) induced NF-κB-dependent transcription of cell adhesion molecules (CAMs) and monocyte adhesion. These effects were prominently enhanced by either pretreatment with the MEK inhibitors, PD98059 and U0126 or overexpression of a dominant negative form of MEK, but blocked by a wild type ERK. Consistently, inhibition of ERK significantly increased IκB kinase (IKK) activity, IκBα phosphorylation, and nuclear translocation of NF-κB induced by VEGF, whereas overexpression of ERK resulted in the loss of these responses to VEGF. Using two PKC inhibitors has demonstrated that VEGF concomitantly stimulates IKK and its negative regulatory signal ERK through PKC that lies downstream of KDR/Flk-1. Strikingly, elevation of ERK in endothelial cells markedly inhibited CAM expression and NF-κB activation as well as monocyte adhesion induced by IL-1β and TNF-α. The data collectively suggest that ERK serves as an anti-inflammatory signal that suppresses expression of NF-κB-dependent inflammatory genes by inhibiting IKK activity in endothelial cells. Measuring the existence of ERK activity in vascular endothelial cells may be useful for predicting the feasibility and potency of inflammatory reactions in the vasculature.

Keywords: VEGF; ERK; NF-κB; CAMs; Inflammation

1. Introduction

Inflammatory conditions are characterized by the migration of proliferating leucocytes from the blood to the tissues and involve a coordinated series of adhesion processes between circulating and resident leukocytes and the vascular endothelium [1–3]. These events are controlled by different types of adhesion molecules on the leukocytes and endothelium [3]. In particular, expression of cell adhesion molecules (CAMs), such as E-selectin, intercellular adhesion molecule-1 (ICAM-1), and vascular cell adhesion molecule-1 (VCAM-1),

Abbreviations: VEGF, vascular endothelial growth factor; HUVECs, human umbilical vein endothelial cells; bFGF, basic fibroblast growth factor; EGF, epidermal growth factor; TNF-α, tumor necrosis factor-α; IL-1β, interleukin-1β; KDR, Flk-1/kinase-insert domain containing receptor; VCAM-1, vascular cell adhesion molecule-1; ICAM-1, intercellular adhesion molecule-1; PI3K, phosphatidylinositol 3′-kinase; PLC, phospholipase C; PKC, protein kinase C; IKK, IκB kinase; MEK, mitogen-activated protein/extracellular signal-regulated kinase kinase; ERK, extracellular signal-regulated kinase; RT-PCR, reverse transcriptase-polymerase chain reaction.

* Corresponding author. Tel.: +82 2 2123 5697; fax: +82 2 362 9897.
E-mail address: ygkwon@yonsei.ac.kr (Y.-G. Kwon).
[1] These authors contributed equally to this study.

0898-6568/$ - see front matter © 2005 Elsevier Inc. All rights reserved.
doi:10.1016/j.cellsig.2005.08.007

on the surface of endothelial cells is required for endothelial–leukocyte cell interaction [1]. In the absence of inflammation, CAM expression is low on the endothelial cells of most vascular beds, but it dramatically increases in response to a number of extracellular stimuli, including tumor necrosis factor-α (TNF-α), interleukin-1β (IL-1β), vascular endothelial growth factor (VEGF), and bacterial lipopolysaccharides [4–6]. Among the classical transcription factors activated by inflammatory cytokines, nuclear factor-κB (NF-κB) plays a pivotal role in the regulation of inflammatory response genes [7,8]. Indeed, it is considered to be a major transcriptional regulator of CAMs in endothelial cells [9].

In mammalian, the five members of the NF-κB family, p65 (RelA), RelB, c-Rel, p50/p105 (NF-κB1), and p52/p100 (NF-κB2), exist in quiescent cells as homo- or heterodimers bound to IκB family proteins and retained in the cytoplasm as an inactive state [10]. In stimulated cells, IκB is degraded through the ubiquitin-proteasome pathway upon specific phosphorylation by activated IκB kinase (IKK) [11]. The IKK activity in cells can be purified as a 700–900-kDa complex, and has been shown to contain two kinase subunits, IKKα (IKK1) and IKKβ (IKK2), and a regulatory subunit, NEMO (NF-κB essential modifier) or IKKγ [11–13]. In the canonical NF-κB signaling pathway, IKKβ is both necessary and sufficient for phosphorylation of IκBα on Ser 32 and Ser 36, and IκBβ on Ser 19 and Ser 23 [12]. By contrast, although the role of IKKα in the canonical pathway is unclear, recent studies suggest that the IKKα subunit phosphorylates p100 and causes its inducible processing to p52 [13].

The activation of the IKK complex is suggested to be exerted by phosphorylation of the IKK complex by the mitogen-activated protein kinase kinase kinase (MAP3K) family including NF-κB-inducing kinase [14], mitogen-activated protein/ERK kinase kinase 1 (MEKK) [15], MEKK3 [16], TGF-β activating kinase 1 [17] and NF-κB-activating kinase [18]. The MAP3K family phosphorylated and induced NF-κB activation when overexpressed or when assayed in vitro, but the mechanism by which cytokines lead to the activation of the IKK complex in vivo is still controversial [19]. Alternatively, previous studies have also suggested that IKK recruitment to receptor complexes at the cell membrane results in its autophosphorylation and subsequent activation [20]. Indeed, IKK recruitment to the TNF receptor-1 complex is shown to be required for TNFα-mediated activation of the IKK complex [11,21–23]. In addition, the important involvement of various intracellular adaptors such as TNF-receptor-associated factors and death-domain kinase receptor-interacting protein in receptor-mediated NF-κB pathway has been extensively reported [24]. However, despite of a large number of studies in vitro and in vivo, the specific upstream signaling mechanism that regulates the IKK activity remains for further investigation.

In the present study, we report an important regulatory role of extracellular signal-related kinase (ERK) in controlling expression of NF-κB-dependent inflammatory genes in vascular endothelial cells. We found that inhibition of ERK markedly increased CAM expression in response to VEGF, which induces both ERK and NF-κB activation in endothelial cells, and this effect was correlated with increased NF-κB activation. Furthermore, elevation of ERK activity in endothelial cells resulted in the suppression of CAM expression and NF-κB activation as well as leukocyte adhesion induced by IL-1β and TNF-α in addition to VEGF. We therefore propose that ERK is a potential intracellular regulator that suppresses vascular inflammation by inhibiting NF-κB activation in endothelial cells.

2. Materials and methods

2.1. Cell culture and reagents

Human umbilical vein endothelial cells (HUVECs) were isolated from human umbilical cord veins by collagenase treatment as described previously [25] and used in passages 2–7. The cells were grown in M199 medium (Invitrogen, Carlsbad, CA) supplemented with 20% fetal bovine serum, 100 units/ml penicillin, 100 μg/ml streptomycin, 3 ng/ml bFGF (Upstate Biotechnology, Lake Placid, NY), and 5 units/ml heparin at 37 °C in humidified 5% CO_2/95% air. U937 cells were grown in RPMI-1640 (Invitrogen). VEGF was from Upstate Biotechnology (Lake Placid, NY), PD98059 from Alexis (San Diego, CA), and U0126 and GF109203X from BIOMOL (Plymouth Meeting, PA). Chelerythrine chloride and actinomycin D were from Sigma. M199, heparin, Trizol reagent and LipofectAMINE Plus were purchased from Invitrogen. Antibodies used were as follows: rabbit anti-VCAM-1 polyclonal antibody, mouse anti-actin monoclonal antibody (Santa Cruz Biotechnology, SantaCruz, Calif), rabbit anti-phospho-IκB-α polyclonal antibody (Cell Signaling, Beverly, MA), mouse anti-phospho-ERK (Thr-202/Tyr-204) monoclonal antibody, and rabbit anti-ERK polyclonal antibody (New England Biolabs, Beverly, MA). All other reagents were purchased from Sigma unless otherwise indicated.

2.2. Construction of reporter plasmids

The VCAM-1 luciferase plasmids were constructed as described previously [26]. The human VCAM-1 promoter, spanning 1716 to +119 bp, was amplified by PCR with primers containing 5′ *KpnI* and 3′ *XhoI* restriction sites. The resulting PCR fragment was digested with *KpnI* and *XhoI* and cloned into pGL3-basic vector (Promega). Synthetic oligonucleotide sense and antisense primers were used to generate a series of DNA fragments with successive 5′ deletions. All PCR products were digested with *KpnI* and *XhoI* and cloned into pGL3-basic vector. The following deletion constructs of the human VCAM-1 promoter were generated: 1716 to +119 bp (fragment 6), 366 to +119 bp (fragment 5), 296 to +119 bp (fragment 4), 210 to +119 bp fragment 3) and 38 to +119 bp (fragment 2). To construct the ICAM-1 luciferase plasmid, we cloned regions spanning −1350 to +45 bp of the human ICAM-1 promoter into pGL3-basic vector (Promega). Plasmid DNAs were purified from bacterial cultures using an Endofree Plasmid Maxi kit (Qiagen, Chatsworth, CA). We confirmed all constructs by restriction enzyme mapping and sequencing.

2.3. Transfections and analysis of luciferase activity

HUVECs were transfected with 1 μg of the above plasmids and 1 μg of the control pCMV-β-gal plasmid using LipofectAMINE Plus reagents (Invitrogen, Carlsbad, CA). Cell extracts were prepared twenty-four hours after transfection, and luciferase assays carried out with the Luciferase Assay System (Promega). Luciferase activities were normalized with respect to parallel β-galactosidase activities, to correct for differences in transfection efficiency, and the β-galactosidase assays were performed using the β-Galactosidase Enzyme Assay System (Promega). Each experimental point was performed in at least quadruplicate.

2.4. Flow cytometry

Cells from subconfluent cultures were detached gently from plates with PBS containing 2 mM EDTA. The cells were washed two or three times with PBS, resuspended in PBS containing 3% bovine serum albumin and incubated with FITC-conjugated VCAM-1 antibody (Serotec) for 30 min on ice. They were then fixed with 2% paraformaldehyde and analyzed by flow cytometry in a fluorescence-activated cell sorter (Becton Dickinson). Each experimental condition was performed in quadruplicate.

2.5. Semi-quantitative RT-PCR analysis

Total RNA was obtained from HUVECs with a TRIzol reagent kit. 0.5–5 μg RNA samples were used in the reverse transcriptase-polymerase chain reactions (RT-PCR), and the correlation between the amounts of RNA used and quantity of PCR products from VCAM-1 mRNA and the internal standard (β-actin) mRNA was examined. Briefly, target RNA was converted to cDNA by treatment with 200 units of reverse transcriptase and 500 ng of oligo(dT) primer in 50 mM Tris–HCl (pH 8.3), 75 mM KCl, 3 mM $MgCl_2$, 10 mM dithiothreitol, and 1 mM dNTPs at 42 °C for 1 h. The reaction was stopped by heating at 70 °C for 15 min. One μl of the cDNA mixture was used for enzymatic amplification. The polymerase chain reaction was performed in 50 mM KCl, 10 mM Tris–HCl (pH 8.3), 1.5 mM $MgCl_2$, 0.2 mM dNTPs, 2.5 units of *Taq* DNA polymerase, and 0.1 μM of primers for VCAM-1. Amplification was performed in a DNA thermal cycler (model PTC-200; MJ Research) under the following condition: denaturation at 94 °C for 5 min for the first cycle and for 30 s thereafter, annealing at 60 °C (VCAM-1), for 30 s, and extension at 72 °C for 30 s for 25 repetitive cycles. Final extension was at 72 °C for 10 min. The primers used for VCAM-1 were as follows: 5′-GATACAACCGTCTTGGTCAGCCC-3′ (sense) and 5′CGC-ATCCTTCAACTGGCCTT-3′ (antisense). Each experimental condition was performed in quadruplicate.

2.6. Transfer vector constructs

HIV-vectors were produced from the previously described SIN-18 vector, which contains a large deletion in the U3 region of the 3′ long terminal repeat (LTR) [27]. The SIN.cPPT.CMV-EGFP-W vector contained the enhanced green fluorescent protein (EGFP) transgene driven by the human cytomegalovirus (CMV) immediate-early enhancer/promoter. The SIN.cPPT.ERK2-EGFP-W vector contained the human extracellular signal-related kinase 2 gene.

2.7. Lentiviral vectors and in vitro gene transfer

VSV-G-pseudotyped, HIV-1-based vector particles were produced by cotransfection of four plasmids (pMDLg/pRRE: 12 μg; pRSVrev: 3 μg; pMD.G: 5 μg, SIN vector: 20 μg) onto 293T cells. Culture medium was replaced by serum-free SFM-II medium (Invitrogen) 15 h post-transfection. Thirty-two hours later, cell supernatants were harvested, filtered through a 0.45 μm filtration system, concentrated on Centricon Plus-80 Biomax MW 100,000 (Millipore, Le-Mont-sur-Lausanne, Switzerland), resuspended in PBS, and re-concentrated on Centricon-20. The titer of the SIN.cPPT.CMV-EGFP-W vector stock solution was 5×10^9 transducing units (TU)/ml by flow cytometry on 293T cells, and 3×10^4 ng p24 antigen per ml by p24-ELISA. The SIN.cPPT.ERK2-EGFP-W vector was titered by flow cytometry on HUVECs (of note, titration of SIN.cPPT.CMV-EGFP-W yielded similar results in HUVECs and 293T cells). HUVECs were seeded in six-well plates and allowed to adhere overnight. Viral vectors were added to cell cultures at varying multiplicities of infection (MOIs ≈1–50). At 18 h, cells were washed and medium was replaced. Cells were harvested at the indicated time points. Percentages of EGFP-positive cells and their mean fluorescence values (MFVs) were determined by flow cytometry (FACScan).

2.8. Preparation of nuclear extracts and electrophoretic mobility shift assays

Cells were washed three times with ice-cold Tris-buffered saline (TBS) and resuspended in 400 μl of buffer A [10 mM HEPES (pH 7.9), 10 mM KCl, 0.1 mM EDTA, 0.1 mM EGTA, 1 mM dithiothreitol (DTT), 1 mM phenylmethylsulfonyl fluoride (PMSF), 5 μg/ml of leupeptin, and 5 μg/ml of aprotinin]. After 15 min, Nonidet P-40 (NP-40) was added to a final concentration of 0.6%. Nuclei were pelleted and suspended in 50 μl of buffer C [20 mM HEPES (pH 7.9), 0.4 M NaCl, 1 mM EDTA, 1 mM EGTA, 1 mM DTT, 1 mM PMSF, 5 μg/ml of leupeptin, and 5 μg/ml of aprotonin]. After 30 min agitation at 4 °C, the lysates were centrifuged, and the supernatants containing the nuclear proteins were diluted with buffer C. Binding reactions contained 15 μg of nuclear protein and a ^{32}P end-labeled, double-stranded oligonucleotide containing the NF-κB binding site on the human VCAM-1 promoter (5′-CCTTGAAGGGATTTCCCTCC-3′) and were incubated for 30 min. Cold competition controls were performed by preincubating the nuclear proteins with a 20-fold molar excess of unlabeled NF-κB double-stranded oligonucleotide for 20 min. The mixtures were resolved on native 5% polyacrylamide gels, which were dried and autoradiographed.

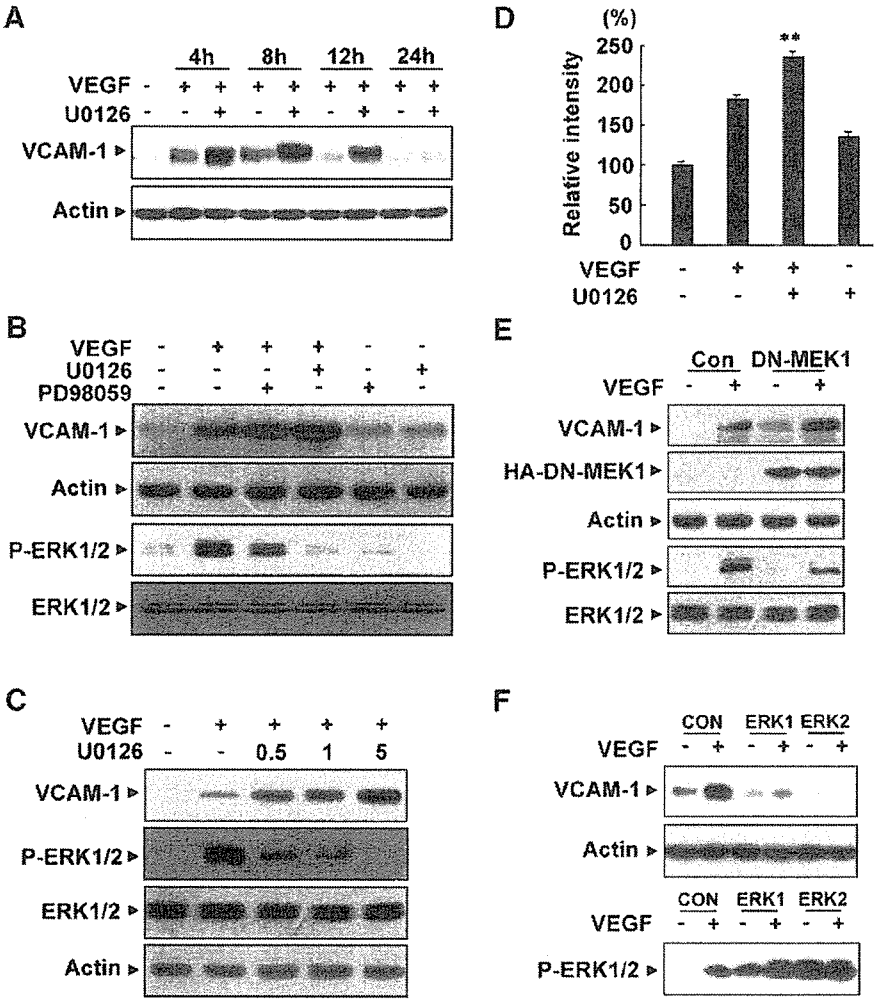

Fig. 1. Inhibition of ERK resulted in increased expression of VCAM-1 in response to VEGF. (A) HUVECs were incubated for 30 min with or without 5 μM U0126 and stimulated with 10 ng/ml VEGF for the indicated times. (B) HUVECs were pretreated for 30 min with 5 μM U0126 or 10 μM PD98059 prior to stimulation with 10 ng/ml VEGF for 10 min (*lower panel*) or 8 h (*upper panel*). (C) HUVECs were incubated for 30 min with or without various concentrations of U0126 and stimulated with 10 ng/ml VEGF for 10 min (*lower panel*) or 8 h (*upper panel*). Western blots were probed with anti-VCAM-1 antibody and an anti-phospho-ERK antibody, and reprobed with anti-actin antibody or anti-ERK antibody to verify equal loading of proteins. (D) HUVECs were pretreated for 30 min with 5 μM U0126 and then stimulated with 10 ng/ml VEGF for 8 h. The cells were detached from the plates, treated with FITC-conjugated VCAM-1 antibody and analyzed with a FACScan. Staining was quantified by flow cytometry. HUVECs were transfected with hemagglutinin (HA) tagged dominant negative form of MEK1, DN-MEK1, (E) or a wild form of ERKs (ERK1, 2) (F) and then stimulated with VEGF (10 ng/ml) for 10 min (*lower panel*) or 8 h (*upper panel*). Western blots were probed with anti-VCAM-1, anti-HA, and anti-phospho-ERK antibody and reprobed with anti-actin antibody or anti-ERK antibody to verify equal loading of proteins. Con indicates cells transfected with empty vector. **, $P<0.01$ versus VEGF alone.

Each experimental point was performed in duplicate and represents several independent conditions.

2.9. In vitro kinase assays

IKK was assayed as described previously [28]. Briefly, the IKK complex was precipitated from whole cell extracts with antibody against IKK-γ, followed by treatment with protein A-Sepharose beads (Pierce). After a 2 h incubation, the beads were washed with lysis buffer and assayed in kinase assay mixture containing 50 mM HEPES (pH 7.4), 20 mM $MgCl_2$, 2 mM dithiothreitol, 20 μCi of [γ-^{32}P]ATP, 10 μM unlabeled ATP, and 2 μg of substrate GST-IκBα (amino acids 1–54). After incubation at 30 °C for 30 min, the reaction was terminated by boiling in SDS sample buffer for 5 min. Finally, the protein was resolved on 10% SDS-PAGE, the gel was dried, and the radioactive bands were visualized with a PhosphorImager. To determine the total amounts of IKK complex in each sample, 50 μg of whole cell protein was resolved on 7.5% SDS-PAGE, electrotransferred to a nitrocellulose membrane, and blotted with anti-IKK-γ antibody. The data represent the average of two separate experiments, each performed in duplicate.

2.10. Immunocytochemical localization of p65

Nuclear translocation of the p65 subunit of NF-κB was examined by an immunocytochemical method as described previously [28]. Briefly, treated cells were fixed with 2%

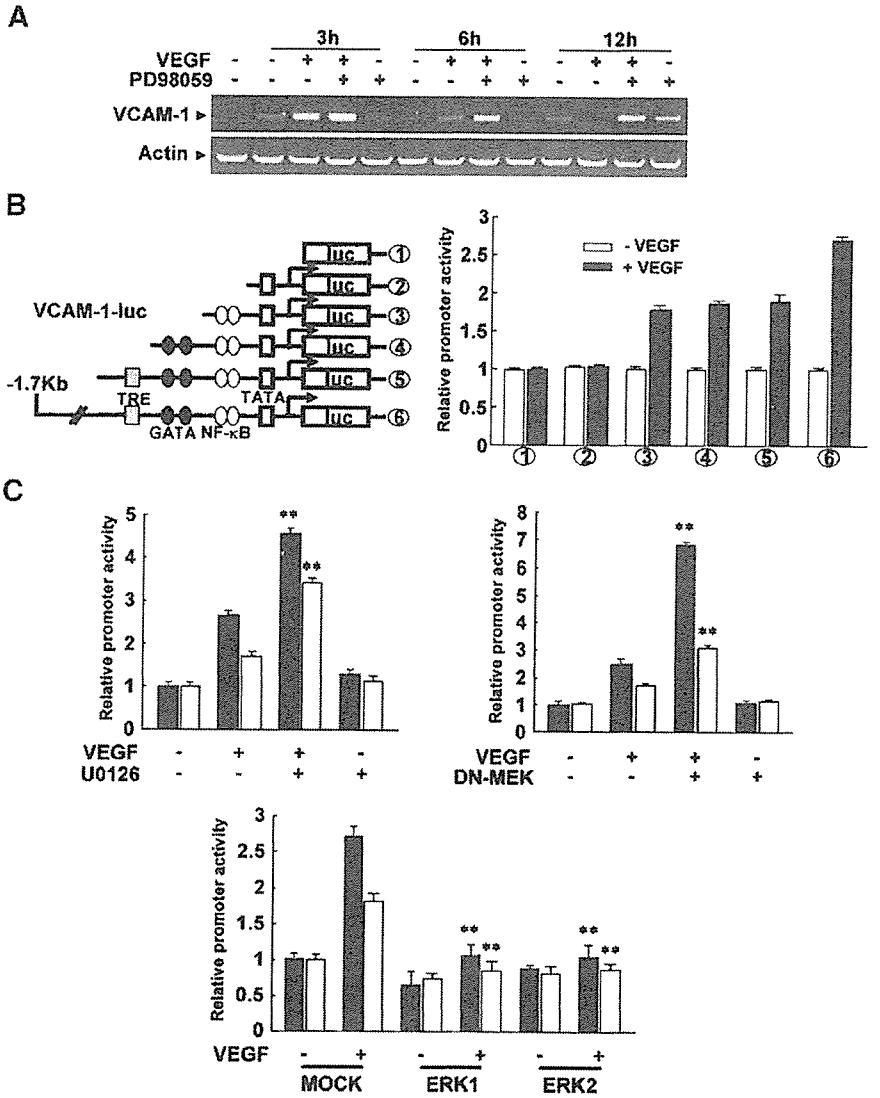

Fig. 2. ERK down-regulates VEGF-induced transcription of VCAM-1 by inhibiting NF-κB. (A) HUVECs were incubated for 30 min with or without 10 μM PD98059 and stimulated with 10 ng/ml VEGF for the indicated times. Total mRNAs were isolated and RT-PCR was performed with specific primers for human VCAM-1 as described in "Materials and methods". Actin served as an internal control. (B) HUVECs were cotransfected with a β-galactosidase plasmid and the various pVCAM-1-Luc deletion constructs as depicted. Twenty four hours later they were stimulated with 10 ng/ml VEGF for 24 h. (C) HUVECs were cotransfected with pVCAM-1-Luc (fragment 6: 1.8 kilobase pair, fragment 3: 329 bp), a β-galactosidase plasmid, and a dominant negative form of MEK1 (DN-MEK1), or wild form of ERKs (ERK1, 2). Twenty four hours after transfection, they were incubated with 10 ng/ml VEGF for 24 h. Luciferase activity was normalized to β-galactosidase activity. Data are means±S.D. of luciferase light units relative to control untreated cells (set at 100%) in quadruplicate experiments. **, $P<0.01$ versus VEGF alone or MOCK+VEGF.

paraformaldehyde and permeabilized with 0.2% Triton X-100. After washing in phosphate-buffered saline, the slides were blocked with 3% bovine serum albumin for 1 h and the cells incubated with goat polyclonal anti-p65 antibody (Santa Cruz Biotechnology, Santa Cruz, CA) (1 : 100). After 2 h at 4 °C the cells were washed and incubated with anti-goat IgG-rhodamine (Santa Cruz) (1 : 100) for 1 h. The cells were then mounted with mounting medium and observed with a fluorescence microscope (Olympus).

2.11. Adhesion assays

HUVECs were plated on 2% gelatin-coated 96-well plates at a density of 1×10^4 cells/well and stimulated with VEGF for 8 h. Human U937 cells were then added (5×10^4 cells/ml, 200 μl/well) to the confluent HUVEC monolayers and incubated for 30 min. Thereafter the cells in the wells were washed out 3 times with PBS, fixed and stained with Diff-Quick (Baxter Healthcare Corp., McGraw Park, IL). The adherent cells in 5 randomly selected optical fields of each well were counted. Each experimental point was performed in duplicate and represents several independent conditions.

2.12. Western blotting

Cell lysates or immunoprecipitates were fractionated by SDS-PAGE and transferred to polyvinyldifluoride membranes. The blocked membranes were incubated with the appropriate

antibody, and the immunoreactive bands were visualized with a chemiluminescent reagent as recommended by Amersham Biosciences, Inc.

2.13. Statistical analysis

Data are presented as means±S.E., and statistical comparisons between groups were performed by 1-way ANOVA followed by Student's *t* test.

3. Results

3.1. Inhibition of ERK resulted in increased expression of VCAM-1 in response to VEGF

Vascular endothelial growth factor (VEGF), a well characterized angiogenic factor, also acts as a proinflammatory cytokine that produces enhanced leukocyte rolling and adhesion and increases endothelial permeability [29,30]. In endothelial cells, it strongly activates ERK and also induces expression of CAMs [31,32] in a NF-κB-dependent mechanism [31]. However, the level of CAM induction in response to VEGF is significantly lower, when compared in parallel, than those by TNF-α and IL-β, which show very little or negligible effect on ERK activation in endothelial cells (data not shown). Thus, it is supposed that the ERK pathway may interfere expression of inflammatory CAMs in response to proinflammatory factors in endothelium. To test this possibility, we first evaluated the role of ERK in VEGF-induced expression of inflammatory response gene such as VCAM-1 by employing MEK inhibitors, PD98059 and U0126, in endothelial cells. Treatment of HUVECs with VEGF enhanced VCAM-1 expression, with a maximum at 8 h (Fig. 1A). In the presence of 5 μM U0126, the effect of VEGF was markedly increased and prolonged up to 24 h (Fig. 1A). To confirm this inhibitory effect, we treated HUVECs with VEGF

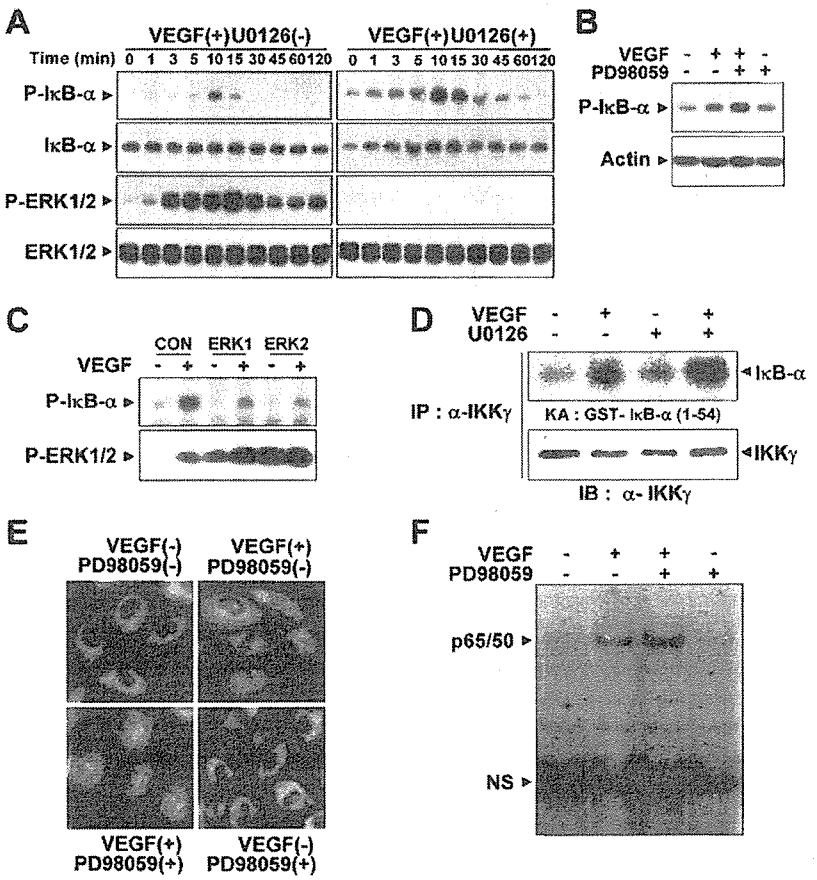

Fig. 3. Inhibition of ERK increases VEGF-induced IKK activity and nuclear translocation of NF-κB. (A) HUVECs were preincubated for 30 min with or without 5 μM U0126 and then stimulated with 10 ng/ml VEGF for the indicated times. Western blots were probed with anti-phospho-IκBα, anti-IκBα, anti-phospho-ERK, and anti-ERK antibodies. (B) HUVECs were preincubated for 30 min with or without 10 μM PD98059 and then stimulated with 10 ng/ml VEGF for 10 min. Western blots were probed with anti-phospho-IκBα and reprobed with an anti-actin antibody to verify equal loading of protein in each. (C) HUVECs were transfected with ERKs wild form (ERK1, 2) and then stimulated with VEGF for 10 min. Western blots were probed with anti-phospho-IκBα, and anti-phospho-ERK antibodies. (D) IKK activity was assessed by immune complex kinase assay as described in "Materials and methods". Recovery of IKK was assessed by immunoblotting for IKK-γ. (E) Immunocytochemical analysis of p65 localization. HUVECs were preincubated for 30 min with or without 10 μM PD98059 and then stimulated with 10 ng/ml VEGF for 30 min and subjected to immunocytochemistry as described in "Materials and methods". (F) HUVECs were preincubated for 30 min with or without 10 μM PD98059 and then stimulated with VEGF (20 ng/ml) for 30 min. Nuclear extracts were isolated and gel shift assay performed with a ^{32}P-radiolabeled NF-κB oligonucleotide of human VCAM-1.

for 10 min in the presence or absence of 5 μM U0126 and measured ERK activity by Western blotting with antibody against the phosphorylated form of ERK1/2 (p44 ERK1 and p42 ERK2). As shown in Fig. 1B, U0126 completely inhibited VEGF-induced ERK activation, whereas VEGF-induced VCAM-1 expression was increased (Fig. 1B). Pretreatment with the other MEK inhibitor, PD98059, also augmented VEGF-induced VCAM-1 expression, while reducing ERK activation (Fig. 1B). U0126 or PD98059 alone had no effect on VCAM-1 expression (Fig. 1B). In addition, the U0126-induced increase in VEGF-induced VCAM-1 expression was dose-dependent, and inversely related to ERK activity (Fig. 1C). FACScan analysis confirmed that U0126 augmented VEGF-induced expression of VCAM-1 on the cell surface of HUVECs (Fig. 1D).

To further confirm that the enhancement of VEGF-induced VCAM-1 expression by the inhibitors was due specifically to inhibition of ERK signaling, we determined the effects of a dominant negative MEK1 (DN-MEK1) mutant and two types of wild type ERK (ERK1 and ERK2). In agreement with the results with chemical inhibitors, Western blot analysis showed that overexpression of DN-MEK1 reduced VEGF-induced ERK phosphorylation, and increased the induction of VCAM-1 by VEGF (Fig. 1E). Moreover, there was a small increase in basal VCAM-1 expression in the cells expressing DN-MEK-1 (Fig. 1E). In contrast, HUVECs overexpressed with either wild type ERK1 or ERK2 increased ERK phosphorylation, and decreased VCAM-1 expression in response to VEGF (Fig. 1F). These results confirm that the ERK pathway inhibits VEGF signaling leading to VCAM-1 expression in endothelial cells.

3.2. ERK down-regulates VEGF-induced transcription of VCAM-1 by inhibiting NF-κB

To determine whether ERK inhibits VEGF-activated transcription of VCAM-1 in endothelial cells, we performed semi-quantitative RT-PCR and assayed transcription from the VCAM-1 luciferase plasmids described in Materials and methods. Treatment of HUVECs with VEGF in the absence of ERK inhibitor induced the appearance of VCAM-1 mRNA within 3 h, and the mRNA declined thereafter (Fig. 2A). In the presence of 10 μM PD98059, the level of VCAM-1 mRNA induced by VEGF was increased and sustained up to 12 h (Fig. 2A). These changes could result either from new synthesis or from increased mRNA stability. Pretreatment with actinomycin D, an inhibitor of transcription, almost completely prevented the increase of VCAM-1 mRNA in response to PD98059 (data not shown), suggesting that ERK inhibits VEGF-activated transcription. The human VCAM-1 promoter (1.7 kb) includes binding sites for NF-κB, TRE, and GATA [26]. Although previous report have implicated NF-κB in VEGF-induced VCAM-1 expression in endothelial cells [26,33], its precise role in activation of the VCAM-1 promoter has not been determined. To identify the cis elements involved, we serially deleted the 1.7 kb VCAM-1 promoter and introduced the resulting plasmids into HUVECs. As shown in Fig. 2B, deletion of the 5′ 1.2 kb region substantially reduced the response to VEGF, but further deletion of the TRE and GATA sites had no appreciable effect. Deletion of the proximal NF-κB binding sites located about 65 and 75 bp upstream of the transcription start site resulted in complete lose of responsiveness to VEGF. These results demonstrate that the NF-κB motifs on the VCAM-1 promoter are important for VEGF-mediated activation of the VCAM-1 promoter, together with an unidentified element in the 5′ 1.2 kb upstream region.

To further confirm the role of ERK in VEGF-induced VCAM-1 transcription, HUVECs were transiently transfected with a VCAM-1 luciferase plasmid harboring the VCAM-1 promoter region. As shown in Fig. 2C, VEGF induced VCAM-1-dependent transcriptional activity, and this was increased by pretreatment with 5 μM U0126, or by introducing DN-MEK-1, but abrogated by ERK or ERK2. These results confirm that ERK controls VEGF-mediated expression of VCAM-1 at the transcriptional level. Since the NF-κB motifs play a significant role in VEGF-induced transcription of VCAM-1, it seemed possible that ERK suppressed activation of NF-κB by VEGF. Indeed, VEGF-induced transcription from a luciferase plasmid containing the proximal NF-κB binding sites of the VCAM-1 promoter was markedly increased by U0126 and DN-MEK1, and almost completely blocked by ERK1 or ERK2 (Fig. 2C). These results suggest that ERK inhibits VEGF-induced transcription of VCAM-1 mRNAs at least in part by suppressing transcription from the NF-κB elements in the VCAM-1 promoter.

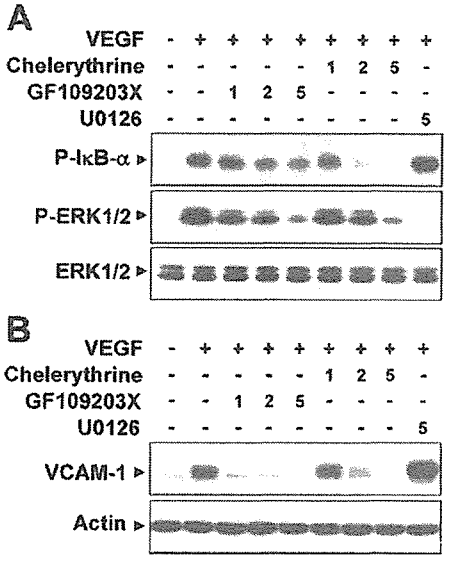

Fig. 4. PKC mediates both IκBα phosphorylation and ERK activation by VEGF. HUVECs were preincubated for 30 min with or without GF109203X, chelerythrine chloride (1, 2, or 5 μM) or 5 μM U0126 and then stimulated with 10 ng/ml VEGF for 10 min (A) or 8 h. (B). Western blots were probed with anti-phospho-IκBα, anti-IκBα, anti-phospho-ERK, and anti-ERK antibodies (A), and anti-VCAM-1 and anti-actin antibodies (B). Actin was used to verify equal loading of protein.

3.3. Inhibition of ERK increases VEGF-induced IKK activity and nuclear translocation of NF-κB

The activated form of NF-κB is a heterodimer that usually consists of two proteins, a p65 (also called relA) subunit and a p50 subunit [7]. In the inactive state, NF-κB is found in the cytoplasm bound to IκBα, which prevents it from entering the nuclei [7,34]. Activation of NF-κB is preceded by the phosphorylation, ubiquitination, and proteolytic degradation of IκBα [34]. Therefore, we examined the effect of ERK inhibitors on VEGF-induced IκBα phosphorylation and degradation by Western blotting with antibodies against phospho-IκBα (Ser-32) and IκBα. As shown in Fig. 3A, VEGF treatment led to phosphorylation of IκBα and maximal activation was observed after 10 min. Pretreatment with U0126 substantially enhanced VEGF-induced IκBα phosphorylation. Moreover, while degradation of IκBα was barely detectable after stimulation with VEGF on its own,

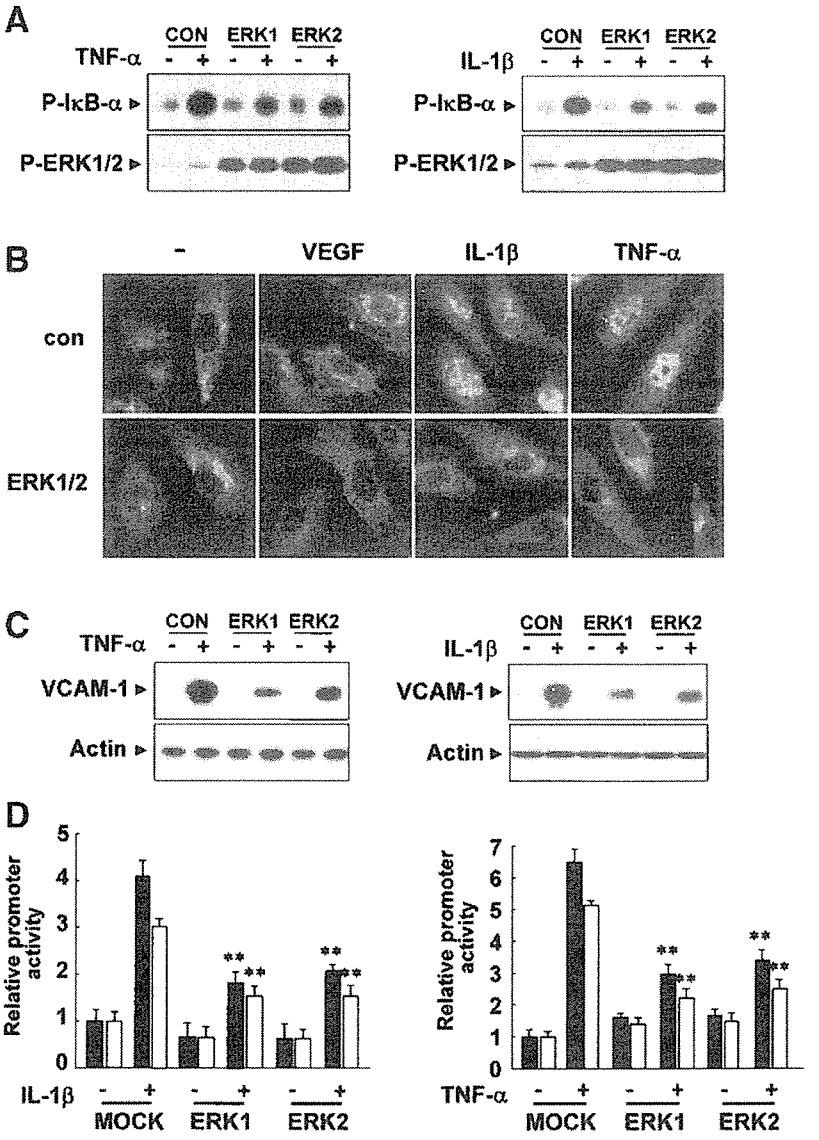

Fig. 5. Overexpression of ERK suppresses NF-κB activation and VCAM-1 expression in response to IL-1β and TNF-α. (A) HUVECs were transfected with ERK wild form (ERK1, 2) and then stimulated with 10 ng/ml TNF-α or 50 units/ml IL-1β for 10 min. Western blots were probed with anti-phospho-IκBα and anti-phospho-ERK antibodies. (B) Immunocytochemical analysis of p65 localization. HUVECs were transfected with ERKs wild form (ERK1, 2) and then stimulated with 10 ng/ml VEGF, 10 ng/ml TNF-α or 50 units/ml IL-1β for 30 min and subjected to immunocytochemistry as described in "Materials and methods". (C) HUVECs were transfected with ERKs wild form (ERK1, 2) and then stimulated with 10 ng/ml TNF-α or 50 units/ml IL-1β for 8 h. Western blots were probed with anti-VCAM-1 and reprobed with an anti-actin antibody to verify equal loading of protein in each. (D) HUVECs were cotransfected with pVCAM-1-Luc (fragment 6: 1.8 kilobase pair, fragment 3: 329 bp), a β-galactosidase plasmid, and a ERKs wild form (ERK1, 2). Twenty four hours after transfection, they were incubated with 10 ng/ml TNF-α or 50 units/ml IL-1β for 24 h. Luciferase activity was normalized to β-galactosidase activity. Data are means±S.D. of luciferase light units relative to control untreated cells (set at 100%) in quadruplicate experiments. **, $P<0.01$ versus MOCK+IL-1β or MOCK+TNF-α.

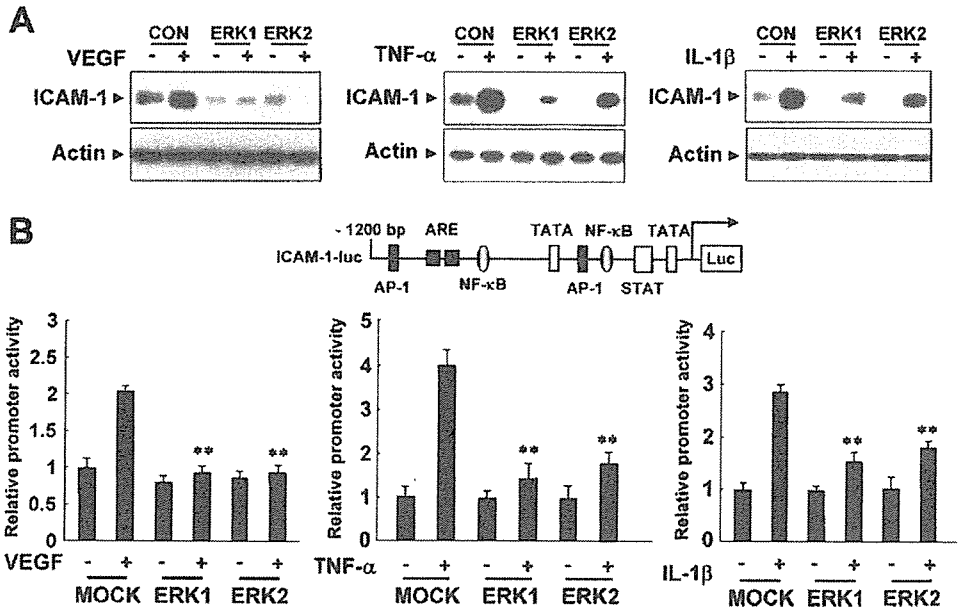

Fig. 6. ERK reduces endothelial ICAM-1 expression in response to VEGF, IL-1β, and TNF-α. (A) HUVECs were transfected with ERKs wild form (ERK1, 2) and then stimulated with 10 ng/ml VEGF, 10 ng/ml TNF-α or 50 units/ml IL-1β for 8 h. Western blots were probed with anti-ICAM-1 and reprobed with an anti-actin antibody to verify equal loading of protein in each. (B) HUVECs were cotransfected with pICAM-1-Luc (1.2 kilobase pair), a β-galactosidase plasmid, and a ERKs wild form (ERK1, 2). Twenty four hours after transfection, they were incubated with 10 ng/ml VEGF, 10 ng/ml TNF-α or 50 units/ml IL-1β for 24 h. Luciferase activity was normalized to β-galactosidase activity. Data are means±S.D. of luciferase light units relative to control untreated cells (set at 100%) in quadruplicate experiments. **, $P<0.01$ versus MOCK+VEGF, MOCK+IL-1β or MOCK+TNFα.

when U0126 was added, the level of IκBα markedly decreased following 30 min of VEGF treatment (Fig. 3A). We also observed that PD98059 increased the effect of VEGF on phosphorylation and subsequent degradation of IκBα in a manner similar to U0126 (Fig. 3B). In contrast, VEGF-induced IκBα phosphorylation was almost completely abrogated by overexpression of ERK1 or ERK2 (Fig. 3C). To further confirm the effect of U0126 on VEGF-induced IκBα phosphorylation, the IκB kinase (IKK) enzymatic assay was performed. IKK is a complex composed of three subunits: IKKα (IKK1), IKKβ (IKK2), and IKKγ (NEMO, IKKAP) [11]. IKK activity was determined in anti-IKKγ immunoprecipitates as described [28]. Cell stimulation with VEGF activated the ability of IKK to phosphorylate GST-IκBα (Fig. 3D). This VEGF-induced IKK activation was significantly increased by pretreatment of U0126 (Fig. 3D).

The dissociation of NF-κB from IκBα results in translocation of NF-κB to the nucleus, where it binds to specific sequences in the promoter regions of target genes. We next determined the effect of ERK inhibitors on VEGF-induced nuclear translocation and NF-κB DNA binding activity. VEGF caused nuclear translocation of the p65 subunit of NF-κB and this was significantly increased by pretreatment with PD98059 (Fig. 3E). Furthermore binding to target NF-κB oligonucleotides was also markedly augmented by pretreatment with PD98059 (Fig. 3F). PD98059 on its own had no effect on nuclear translocation and NF-κB DNA binding activity (Fig. 3E and F). Collectively, these results suggest that ERK suppresses VEGF-induced NF-κB activation by blocking the VEGF signaling pathway leading to IκBα phosphorylation.

3.4. PKC mediates both IκBα phosphorylation and ERK activation by VEGF

Our data indicate that VEGF induces both IκBα phosphorylation and ERK activation in endothelial cells. It was of interest to identify the upstream signaling molecules that lead to IKK and ERK activation. A previous study suggested the involvement of PKC in NF-κB activation leading to endothelial CAM expression [31,35,36]. We therefore examined the role of PKC in IκBα phosphorylation by employing two PKC inhibitors, GF109203X and chelerythrine chloride, and, in parallel, compared the effect of these inhibitors on VEGF-induced ERK activation. As shown in Fig. 4A, both IκBα phosphorylation and ERK activation in response to VEGF were inhibited by GF109203X and chelerythrine chloride, indicating that PKC lies upstream of both IKK and ERK. Under the same condition, U0126 completely inhibited ERK activation in response to VEGF, and increased the VEGF effect on IκBα phosphorylation (Fig. 4A). Similarly, VEGF-induced VCAM-1 expression was blocked by GF109203X and chelerythrine chloride, but increased by U0126 (Fig. 4B). These results suggest that in the VEGF signaling pathway PKC provides a positive signal activating IKK and ERK, a negative signal.

3.5. Overexpression of ERK suppresses NF-κB activation and VCAM-1 expression in response to IL-1β and TNF-α

The role of ERK pathway in other cytokine-induced NF-κB activation was explored. Unlikely to VEGF, IL-1β and TNF-α

did not significantly induce ERK activation in HUVECs in contrast to their strong stimulatory activity on NF-κB. Consistently, inhibition of ERK by pretreatment of HUVECs with 5 μM U0126 did not further increase IκBα phosphorylation in response to either IL-1β or TNF-α (data not shown). However, overexpression of either wild type ERK1 or ERK2 markedly reduced both IL-1β-and TNF-α-induced IκBα phosphorylation (Fig. 5A). In addition, nuclear translocation of p65 subunit of NF-κB induced by either IL-1β or TNF-α was blocked by overexpression of ERKs (Fig. 5B). In agreement, both IL-1β and TNF-α increased endothelial VCAM-1 expression in a NF-κB dependent manner as shown in a promoter assay and these responses were significantly abrogated by overexpression of either ERK1 or ERK2 (Fig. 5C and D). These results raised the possibility that ERK negatively regulates NF-κB-dependent gene expression in endothelial cells through inhibiting the IκBα phosphorylation pathway stimulated by various agonists.

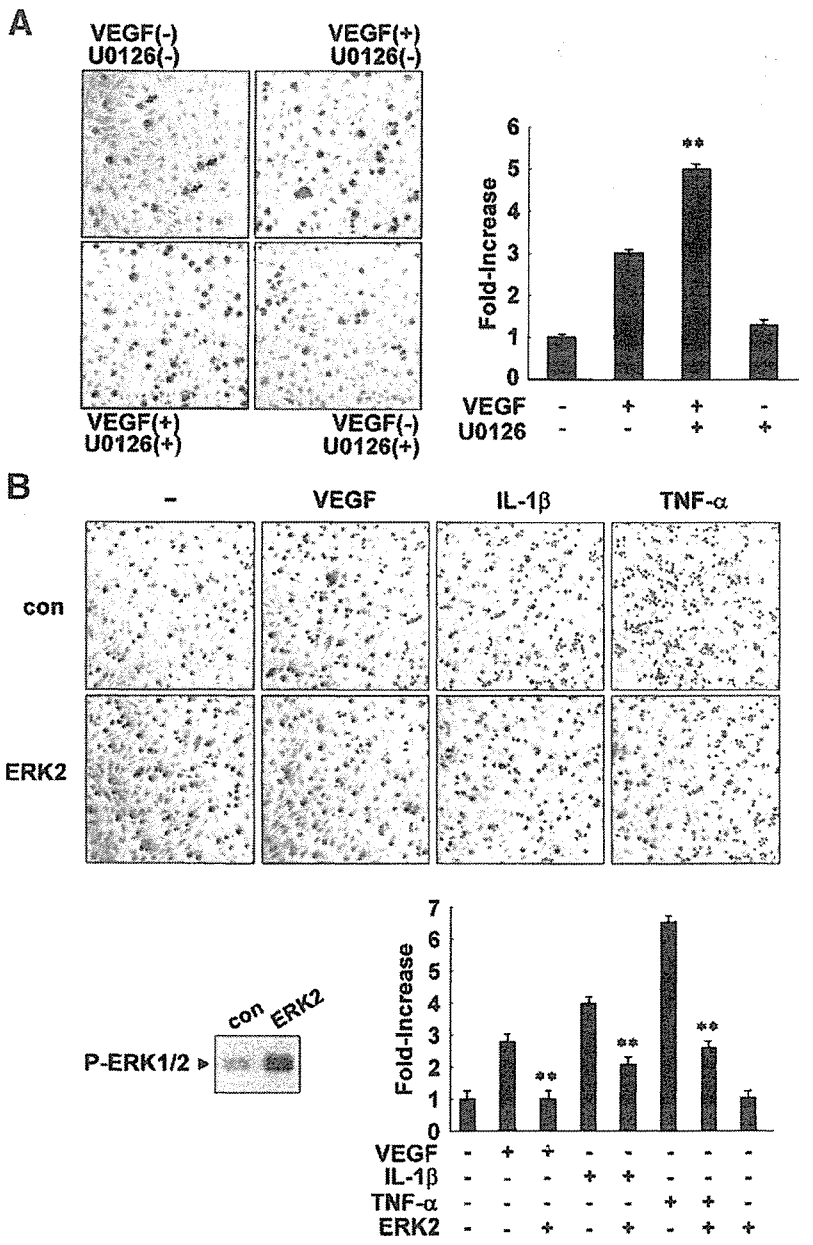

Fig. 7. ERK inhibitors increase VEGF-Induced leukocyte adhesion to endothelial cells. (A) HUVECs were preincubated for 30 min with or without 5 μM U0126 and then stimulated with 10 ng/ml VEGF for 8 h. (B) ERK2 lentiviral vectors were added to cell cultures at varying multiplicities of infection (MOIs ≈1–50). At 18 h, cells were washed and medium was replaced. HUVECs were stimulated with 10 ng/ml VEGF, 10 ng/ml TNF-α or 50 units/ml IL-1β for 8 h. Thereafter adhesion to U937 human monocytes was measured as described in "Materials and methods." Data are means±S.D. of adhesion relative to control untreated cells (set at 100%) in quadruplicate experiments. **, $P<0.01$ versus VEGF, IL-1β or TNF-α.

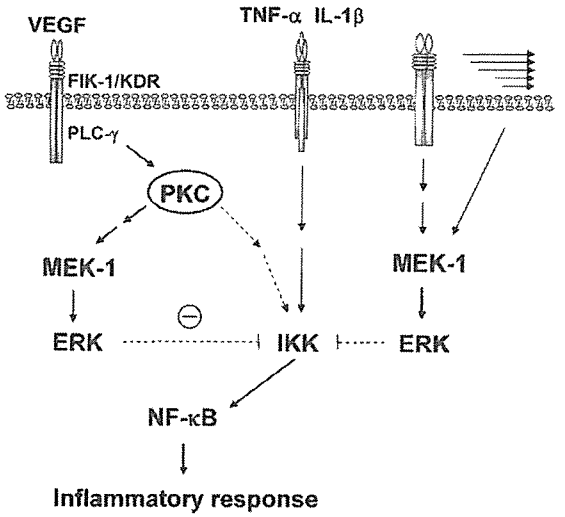

Fig. 8. Potential mechanism supporting anti-inflammatory role of ERK in the vascular wall.

3.6. ERK reduces endothelial ICAM-1 expression in response to VEGF, IL-1β, and TNF-α

We further confirmed the role of ERK pathway on expression of other inflammatory genes in endothelial cells. ICAM-1 is one of representative endothelial cell adhesion molecules expressed in a NF-κB dependent mechanism. As expected, the protein level of ICAM-1 on HUVECs was increased by either treatment of VEGF, IL-1β or TNF-α (Fig. 6A). All these increases were almost completely or markedly inhibited by overexpression of either ERK1 or ERK2 (Fig. 6A). Consistently, ICAM-1-dependent transcriptional activities induced by these cytokines were inhibited by overexpression of ERK1 or ERK2 (Fig. 6B).

3.7. ERK inhibitors increase VEGF-Induced leukocyte adhesion to endothelial cells

Expression of CAMs, such as ICAM-1 and VCAM-1, on the surface of endothelial cells is required for endothelial–leukocyte interaction. Since inhibition of the ERK pathway increases the effect of VEGF on endothelial CAM expression, we tested whether the ERK inhibitor stimulates leukocyte adhesion to endothelial cells. HUVECs were exposed to 10 ng/ml VEGF for 8 h and then co-cultured with human monocytic U937 cells for an additional 1 h. As shown in Fig. 7, the adhesion of U937 cells to HUVECs was increased by VEGF, and this effect was accentuated by pretreatment with 5 μM U0126 (Fig. 7A). U0126 alone, on the other hand, had no effect (Fig. 7A). In contrast, overexpression of ERK2 markedly reduced VEGF-induced adhesion of U937 cells to HUVECs (Fig. 7B). Moreover, both IL-1β-and TNF-α-induced monocyte–endothelial cell interaction was also significantly reduced by overexpression of ERK2 (Fig. 7B).

4. Discussion

Unveiling of endothelial NF-κB activation is pivotal for understanding the inflammatory reaction and the pathogenesis of inflammatory vascular diseases. A large number of studies have revealed the presence of a number of cellular stimuli, including inflammatory cytokines and oscillating shear stress, that lead to the endothelial NF-κB activation [10,37]. Conversely, factors such as angiopoietin-1, bFGF, hepatocyte growth factor (HGF), and normal lamina shear stress were shown to suppress NF-κB activation [38,39]. However, despite of a number of reports, precise understanding of their action mechanisms in the vasculature remains still unclear. Importantly, the present study demonstrates the novel role of ERK in controlling endothelial NF-κB activation and inflammatory gene expression.

Our data showed that inhibition of ERK increased VCAM-1 expression in response to VEGF stimulation, but that ERK inhibitors alone had no significant effect. This indicates that inhibition of ERK itself is incapable of stimulating VCAM-1 expression in endothelial cells, and suggests that VEGF sets in train both positive and negative signals related to VCAM-1 expression and that ERK may serve as an internal suppressor of the positive signal. Using two PKC inhibitors, it is clearly demonstrated that VEGF stimulates both ERK and IKK through PKC that lies downstream of KDR/Flk-1. Since ERK inhibits IKK activation by VEGF (Fig. 4), PKC seems to transmit both positive and negative signals involved in IKK activation. Therefore, the relatively weak activation of IKK and expression of inflammatory genes by VEGF is likely to be due to the concomitant activation of ERK. Similar phenomenon was observed in TNF-related activation-induced cytokine (TRANCE)-induced NF-κB activation and VCAM-1 expression. TRANCE stimulated ERK, IκBα phosphorylation, and transcriptional activity of NF-κB in HUVECs [40,41]. Pretreatment of the ERK inhibitors significantly enhanced TRANCE-induced NF-κB activation and VCAM-1 expression (data not shown), suggesting the suppressive role of concomitantly activated ERK in the cytokine-induced NF-κB pathway in endothelial cells.

Unlikely to VEGF, IL-1β and TNF-α had little effect on ERK activation in HUVECs, but they much strongly induced IKK activation and VCAM-1 expression compared to VEGF. The effects of IL-1β and TNF-α on IKK activation and VCAM-1 expression was very slightly increased by the ERK inhibitor (data not shown) but markedly suppressed by overexpression of ERK1 or ERK2. We also tested the effect of bFGF and EGF on VCAM-1 expression in HUVECs. These two growth factors markedly stimulated ERK activation in HUVECs, but did not induce VCAM-1 expression. In addition, ERK inhibitors had no significant effect on VCAM-1 expression (data not shown), presumably because these growth factors do not activate the NF-κB signaling pathway. We have recently reported that HGF counteracts VEGF-induced endothelial CAM expression through inhibiting IKK-mediated NF-κB activation [42]. HGF itself was unable to induce NF-κB activation but strongly stimulated ERK activation in endothelial cells (data not shown).

In deed, it is observed that pretreatment of the ERK inhibitor prior to HGF administration results in reversing the inhibitory effect of HGF on VEGF-induced IκBα phosphorylation and VCAM-1 expression (data not shown). Although the precise mechanism engaged in agonists-dependent activation or inhibition of NF-κB pathway remains elusive, it is at least in part suggested that the cellular level of ERK activity may be one of crucial components to control IKK-mediated NF-κB activation in endothelial cells. Western blotting with antibodies against phospho-IκBα (Ser-32) and IκBα revealed that the ERK inhibitors increase IκBα phosphorylation at Ser-32 and degradation in response to VEGF (Fig. 4). Conversely, forced elevation of ERK activity in HUVECs resulted in the inhibition of phosphorylation of IκBα on Ser-32 by VEGF, IL-1β, and TNF-α. IKK exists as a high molecular complex containing two kinase subunits, IKKα (IKK1) and IKKβ (IKK2), and a regulatory subunit, NEMO [13]. The phosphorylation of IκBα on Ser-32 and Ser-36 is mediated mainly by the kinase activity of IKKβ and led to its proteolytic degradation and subsequent nuclear translocation of NF-κB [13]. Therefore, ERK is most likely to inhibit the canonical NF-κB pathway that involves IKK-mediated IκBα phosphorylation in endothelial cells.

In conclusion, our present data apparently demonstrate a novel function of ERK as a curb of endothelial NF-κB activation with possible mechanism (Fig. 8). Indeed, elevation of ERK activity in endothelial cells significantly suppressed expression of NF-κB-dependent genes such as ICAM-1 and VCAM-1 in response to cytokine stimulation. These effects were functionally correlated with decreased endothelial cell–monocyte interaction. Although the further study is required to prove the anti-inflammatory nature of ERK in more complex in vivo environment, our findings suggest that ERK activity constitutively or transiently induced by normal laminar flow or various endothelial stimuli may serve as a negative regulator of vascular inflammation by suppressing endothelial NF-κB activation. Therefore, measuring the existence of ERK activity in vascular endothelial cells may be useful for predicting the feasibility and potency of inflammatory reactions in the vascular wall.

Acknowledgments

This work was supported by a Next Generation Growth Engine Program Grant and Vascular System Research Center Grant from the Korean Ministry of Science and Technology.

References

[1] H. Ulbrich, E.E. Eriksson, L. Lindbom, Trends Pharmacol. Sci. 24 (2003) 640.
[2] D. Vestweber, Curr. Opin. Cell Biol. 14 (2002) 587.
[3] W.A. Muller, Lab Invest. 82 (2002) 521.
[4] P. Xia, J.R. Gamble, K.A. Rye, L. Wang, C.S. Hii, P. Cockerill, Y. Khew-Goodall, A.G. Bert, P.J. Barter, M.A. Vadas, Proc. Natl. Acad. Sci. U. S. A. 95 (1998) 14196.
[5] K.T. Piercy, R.L. Donnell, S.S. Kirkpatrick, C.H. Timaran, S.L. Stevens, M.B. Freeman, M.H. Goldman, J. Surg. Res. 105 (2002) 215.
[6] S. Zeuke, A.J. Ulmer, S. Kusumoto, H.A. Katus, H. Heine, Cardiovasc. Res. 56 (2002) 126.
[7] J. Peter, D.M. Barnes, Sc. D, Michael Karin, N. Engl. J. Med. 336 (1997) 1066.
[8] P.A. Baeuerle, T. Henkel, Annu. Rev. Immunol. 12 (1994) 141.
[9] C. Maaser, S. Schoeppner, T. Kucharzik, M. Kraft, E. Schoenherr, W. Domschke, N. Luegering, Clin. Exp. Immunol. 124 (2001) 208.
[10] J.T. Wu, J.G. Kral, J. Surg. Res. 123 (2005) 158.
[11] Y. Yamamoto, R.B. Gaynor, Trends Biochem. Sci. 29 (2004) 72.
[12] P. Viatour, M.P. Merville, V. Bours, A. Chariot, Trends Biochem Sci. 30 (2005) 43.
[13] M.S. Ayden, S. Hosh, Genes Dev. 18 (2004) 2195.
[14] E. Majewska, E. Paleolog, Z. Baj, U. Kralisz, M. Feldmann, H. Tchorzewski, Scand. J. Immunol. 45 (1997) 385.
[15] H. Zhang, A.C. Issekutz, Am. J. Pathol. 160 (2002) 2219.
[16] M. Kaneki, S. Kharbanda, P. Pandey, K. Yoshida, M. Takekawa, J.R. Liou, R. Stone, D. Kufe, Mol. Cell. Biol. 19 (1999) 461.
[17] R. Datta, K. Yoshinaga, M. Kaneki, P. Pandey, D. Kufe, J. Biol. Chem. 275 (2000) 41000.
[18] J.H. Je, J.Y. Lee, K.J. Jung, B. Sung, E.K. Go, B.P. Yu, H.Y. Chung, FEBS Lett. 566 (2004) 183.
[19] C. Schmidt, B. Peng, Z. Li, G.M. Sclabas, S. Fujioka, J. Niu, M. Schmidt-Supprian, D.B. Evans, J.L. Abbruzzese, P.J. Chiao, Mol. Cell. 12 (2003) 1287.
[20] J.R. Burke, J. Strnad, Biochem. Biophys. Res. Commun. 293 (2002) 1508.
[21] P.E. Hughes, M.W. Renshaw, M. Pfaff, J. Forsyth, V.M. Keivens, M.A. Schwartz, M.H. Ginsberg, Cell 88 (1997) 521.
[22] R. Gum, H. Wang, E. Lengyel, J. Juarez, D. Boyd, Oncogene 14 (1997) 481.
[23] D. Besser, M. Presta, Y. Nagamine, Cell Growth Differ. 6 (1995) 1009.
[24] E. Meylan, F. Martinon, M. Thome, M. Gschwendt, J. Tschopp, EMBO Rep. 3 (2002) 1201.
[25] E.A. Jaffe, R.L. Nachman, C.G. Becker, C.R. Minick, J. Clin. Invest. 52 (1973) 2745.
[26] T. Minami, W.C. Aird, J. Biol. Chem. 276 (2001) 47632.
[27] D. Cefai, E. Simeoni, K.M. Ludunge, R. Driscoll, L.K. von Segesser, L. Kappenberger, G. Vassalli, J. Mol. Cell. Cardiol. 38 (2005) 333.
[28] Y. Takada, A. Mukhopadhyay, G.C. Kundu, G.H. Mahabeleshwar, S. Singh, B.B. Aggarwal, J. Biol. Chem. 278 (2003) 24233.
[29] M.A. Proescholdt, S. Jacobson, N. Tresser, E.H. Oldfield, M.J. Merrill, J. Neuropathol. Exp. Neurol. 61 (2002) 914.
[30] S.D. Croll, J.H. Goodman, H.E. Scharfman, Adv. Exp. Med. Biol. 548 (2004) 57.
[31] I. Kim, S.O. Moon, S.H. Kim, H.J. Kim, Y.S. Koh, G.Y. Koh, J. Biol. Chem. 276 (2001) 7614.
[32] I. Kim, S.O. Moon, S.K. Park, S.W. Chae, G.Y. Koh, Circ. Res. 89 (2001) 477.
[33] H.J. Park, Y.W. Lee, B. Hennig, M. Toborek, Nutr. Cancer 41 (2001) 126.
[34] V. Dixit, T.W. Mak, Cell 111 (2002) 615.
[35] K. Page, J. Li, L. Zhou, S. Iasvovskaia, K.C. Corbit, J.W. Soh, I.B. Weinstein, A.R. Brasier, A. Lin, M.B. Hershenson, J. Immunol. 170 (2003) 5681.
[36] T. Minami, M.R. Abid, J. Zhang, G. King, T. Kodama, W.C. Aird, J. Biol. Chem. 278 (2003) 6976.
[37] G.P. Sorescu, M. Sykes, D. Weiss, M.O. Platt, A. Saha, J. Hwang, N. Boyd, Y.C. Boo, J.D. Vega, W.R. Taylor, H. Jo, J. Biol. Chem. 278 (2003) 31128.
[38] E. Eng, B.J. Ballermann, Microvasc. Res. 65 (2003) 137.
[39] B.H. Jeon, F. Khanday, S. Deshpande, A. Haile, M. Ozaki, K. Irani, Circ. Res. 92 (2003) 586.
[40] Y.M. Kim, Y.M. Kim, Y.M. Lee, H.S. Kim, J.D. Kim, Y. Choi, K.W. Kim, S.Y. Lee, Y.G. Kwon, J. Biol. Chem. 277 (2002) 6799.
[41] J.K. Min, Y.M. Kim, S.W. Kim, M.C. Kwon, Y.Y. Kong, I.K. Hwang, M. H. Won, J. Rho, Y.G. Kwon, J. Immunol. 175 (2005) 531.
[42] J.K. Min, Y.M. Lee, J.H. Kim, Y.M. Kim, S.W. Kim, S.Y. Lee, Y.S. Gho, G.T. Oh, Y.G. Kwon, Circ. Res. 96 (2005) 300.

Oncogene (2006) 00, 1–10

www.nature.com/onc

ORIGINAL ARTICLE

Involvement of adaptor protein Crk in malignant feature of human ovarian cancer cell line MCAS

H Linghu[1,5], M Tsuda[1,2], Y Makino[1,2], M Sakai[1,2], T Watanabe[1,2], S Ichihara[1,2], H Sawa[1,2,4], K Nagashima[1,2], N Mochizuki[3] and S Tanaka[1,2]

[1]Laboratory of Molecular and Cellular Pathology, Hokkaido University Graduate School of Medicine, Sapporo, Hokkaido, Japan; [2]CREST, Japan Science and Technology Cooporation, Saitama, Japan; [3]National Cardiovascular Center Research Institute, Osaka, Japan and [4]21st Century COE Program for Zoonosis Control, Japan

Signaling adaptor protein Crk regulates cell motility and growth through its targets Dock180 and C3G, those are the guanine-nucleotide exchange factors (GEFs) for small GTPases Rac and Rap, respectively. Recently, overexpression of Crk has been reported in various human cancers. To define the role for Crk in human cancer cells, Crk expression was targeted in the human ovarian cancer cell line MCAS through RNA interference, resulting in the establishment of three Crk knockdown cell lines. These cell lines exhibited disorganized actin fibers, reduced number of focal adhesions, and abolishment of lamellipodia formation. Decreased Rac activity was demonstrated by pull-down assay and FRET-based time-lapse microscopy, in association with suppression of both motility and invasion by phagokinetic track assay and transwell assay in these cells. Furthermore, Crk knockdown cells exhibited slow growth rates in culture and suppressed anchorage-dependent growth in soft agar. Tumor forming potential in nude mice was attenuated, and intraperitoneal dissemination was not observed when Crk knockdown cells were injected into the peritoneal cavity. These results suggest that the Crk is a key component of focal adhesion and involved in cell growth, invasion, and dissemination of human ovarian cancer cell line MCAS.

Oncogene (2006) **0**, 000–000. doi:10.1038/sj.onc.1209398

Keywords: ▮; ▮; ▮; ▮

Introduction

The regulation of cell motility is a well-organized process in which cells receive information from the surrounding environment through the extracellular matrix (ECM) (Gumbiner, 1996; Lauffenburger and Horwitz, 1996; Sheetz *et al.*, 1998). Cell surface receptor molecules for the ECM, such as integrins, transmit signals to the actin cytoskeleton through the focal adhesion complex (Brugge, 1998; O'Neill *et al.*, 2000). Tyrosine kinases, such as focal adhesion kinase (FAK) or proline-rich tyrosine kinase 2 (PYK2), are activated by the ECM and their substrates, $p130^{Cas}$ (Crk associated substrate) or paxillin, may play a role in regulation of focal adhesion (Yano *et al.*, 2000; Summy and Gallick, 2003). Downstream of focal adhesion complexes, the Rho family of small GTPases, including Rho, Rac and Cdc42, regulate the reorganization of actin fibers to form stress fibers, lamellipodia and filopodia, all of which control cell motility (Hall, 1998). Although the deregulation of focal adhesion complexes may contribute to motility and invasion of tumor cells, the precise mechanism is not well understood.

Signaling adaptor protein Crk (CT10 regulated kinase), which is mostly composed of SH2 (src homology 2) and SH3 domains, was originally isolated as an avian sarcoma virus CT10 (chicken tumor 10) encoding oncogene product (Mayer *et al.*, 1988). Since the isolation of mammalian homologues of viral Crk, such as c-Crk-I and c-Crk-II (Matsuda *et al.*, 1992b), Crk has been shown to transmit signals under various stimuli including epidermal growth factor, neurotrophic growth factor and fibroblast growth factor (Tanaka *et al.*, 1993; Feller, 2001). c-Crk-II possesses one SH2 domain at the N-terminus and two SH3 domains, wheras its alternative splicing product c-Crk-I is composed of the SH2 domain and a single SH3 domain. The SH2 domain is responsible for binding to the tyrosine phosphorylated form of 130^{Cas} and paxillin, suggesting a role for Crk in regulation of the cytoskeleton (Feller, 2001). In fact, Crk has been shown to transmit signals to small GTPases by association with its downstream effectors such as Dock180 and C3G, which

Correspondence: Dr S Tanaka, Laboratory of Molecular and Cellular Pathology, Hokkaido University School of Medicine, N 15, W 7, Kita-ku, Sapporo, Hokkaido 060-8638, Japan.
E-mail: tanaka@med.hokudai.ac.jp or sitanaka@patho2.med.hokudai.ac.jp
[5]Current address: Department of Obstetrics & Gynecology, First Affiliated Hospital of Chongqing University of Medical Sciences, Chongqing 400012, China.
Received 31 July 2005; revised 28 November 2005; accepted 28 November 2005

Gml : Ver 6.0
Template: Ver 6.1

Journal: ONC ☐ Disk used Despatch Date: 19/1/2006
Article : npg_onc_2004-1264 Pages: 1–10 OP: Solly ED: Viji

are the guanine-nucleotide exchange factors (GEFs) for Rac and Rap, respectively (Tanaka *et al.*, 1994; Gotoh *et al.*, 1995; Hasegawa *et al.*, 1996; Kiyokawa *et al.*, 1998). The activation of Rho was also reported (Tsuda *et al.*, 2002; Iwahara *et al.*, 2003).

Dock180 and its binding molecule ELMO cooperatively regulate Rac activity and are thought to be involved in the phagocytosis of apoptotic cells (Albert *et al.*, 2000; Gumienny *et al.*, 2001; Brugnera *et al.*, 2002). C3G regulates the MAP kinase and JNK pathway by activating Rap and R-Ras, respectively, following phosphorylation on tyrosine residue 504 (Tanaka *et al.*, 1997; Tanaka and Hanafusa, 1998; Mochizuki *et al.*, 2000). Studies in C3G knockout mice suggested a role for C3G in the control of cell adhesion (Ohba *et al.*, 2001).

The contribution of c-Crk to tumorigenesis was suggested by an earlier study showing that c-Crk-I induced anchorage-independent growth of rodent fibroblasts together with tyrosine-phosphorylation of p130^{Cas} (Matsuda *et al.*, 1992b). We previously reported that Crk is overexpressed in human cancers including various carcinomas and sarcomas (Nishihara *et al.*, 2002c). In addition, there are several reports describing overexpression of c-Crk-I in malignant brain tumors and lung cancers (Miller *et al.*, 2003; Takino *et al.*, 2003). Because ovarian cancer possesses prominent metastatic potential in general and frequently exhibit intraperitoneal dissemination in patients, the human ovarian cancer cell line MCAS provides an appropriate model system to study the role of Crk in tumorigenesis (Judson *et al.*, 1999; Chen *et al.*, 2001).

In Crk knockdown MCAS cells, disorganization of actin cytoskeleton and decrease of Rac activity was observed. Cell motility and invasion were also decreased in addition to the growth suppression. Crk knockdown MCAS cells lost the ability of intraperitoneal dissemination in mice. These results suggest that Crk may be involved in malignant feature of human ovarian cancer cell line MCAS.

Results

Association of Crk and its targets in MCAS cells

Because both p130^{Cas} and paxillin are major targets of the SH2 domain of Crk, the tyrosine-phosphorylation status of these proteins was examined in MCAS cells. Immunoprecipitation analysis demonstrated that p130^{Cas} and paxillin were significantly tyrosine-phosphorylated (Figure 1a), and their association with Crk was clearly demonstrated (Figure 1b). We also analysed the association of Crk and its well-known downstream effectors, including Dock180, C3G, Sos and c-Abl, by GST pull-down assay. GST-Crk-I, GST-Crk-II and GST-Crk-SH3(N) associated with these molecules in MCAS cell lysates, whereas GST alone or GST-SH2 did not (Figure 1c).

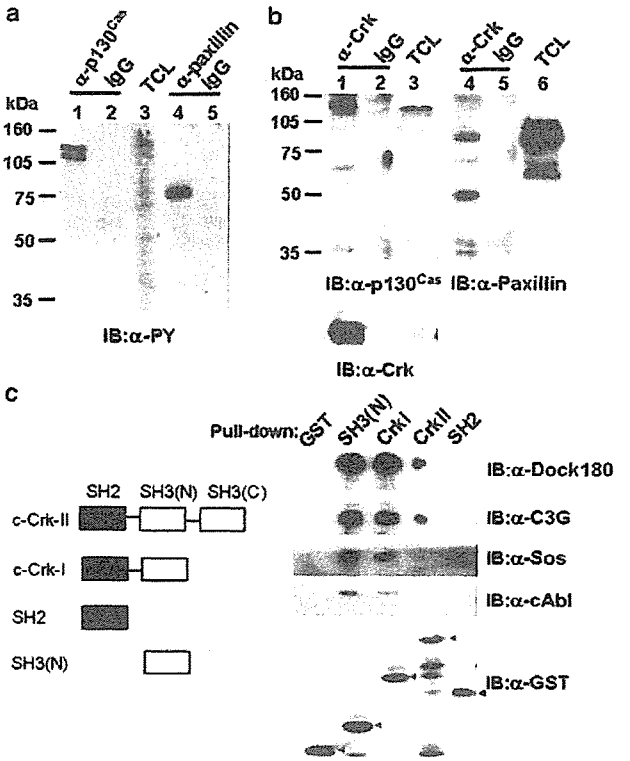

Figure 1 (a) Tyrosine phosphorylation of p130Cas and paxillin in MCAS cells. Immunoprecipitation by using anti-p130^{Cas} Ab (lane 1), antipaxillin Ab (lane 4) or control immunoglobulin (IgG, lanes 2 and 5) was performed, and probed with antiphosphotyrosine Ab. TCL, total cell lysates (lane 3). (b) Association of Crk with p130^{Cas} and paxillin. Immunoprecipitation by using anti-Crk Ab (lanes 1 and 4) or control IgG (lanes 2 and 5) was performed and probed with anti-p130^{Cas} Ab (left panel), antipaxillin Ab (right panel) or anti-Crk Ab (lower panel). (c) Association of Crk and target molecules. MCAS cell lysates were incubated with GST alone or GST fusion form of N-terminus SH3 domain of c-Crk-II (Crk-SH3(N)), c-Crk-I (CrkI), c-Crk-II (CrkII) or SH2 domain of c-Crk-II (SH2), and probed with anti-Dock180, anti-C3G, anti-Sos, anti-Abl or anti-GST Abs. Arrowheads show the calculated molecular weight of the GST fusion proteins.

Establishment of Crk knockdown MCAS cell lines and morphological analysis

To reduce expression of endogenous Crk in MCAS cells, small interfering RNA (siRNA) was employed. By using Crk siRNA in the pSUPER vector, we successfully established three independent Crk knockdown MCAS cell lines, which were designated Crki-1, Crki-2 and Crki-3. In all three cell lines, the expression of c-Crk-I was completely suppressed (Figure 2A). The expression of c-Crk-II was significantly decreased in Crki-1 and Crki-2 cells, whereas it was slightly suppressed in Crki-3 cells (Figure 2A). Endogenous protein levels of CrkL were unchanged as were those of actin (Figure 2A). The tyrosine-phosphorylation levels of p130^{Cas} and paxillin seemed to be slightly different but were statistically constant in Crk knockdown cells (Figure 2B).

In MCAS cells, filopodia and lamellipodia were readily identified at the cell edge (Figure 2C). In contrast, Crk knockdown cells tended to form small

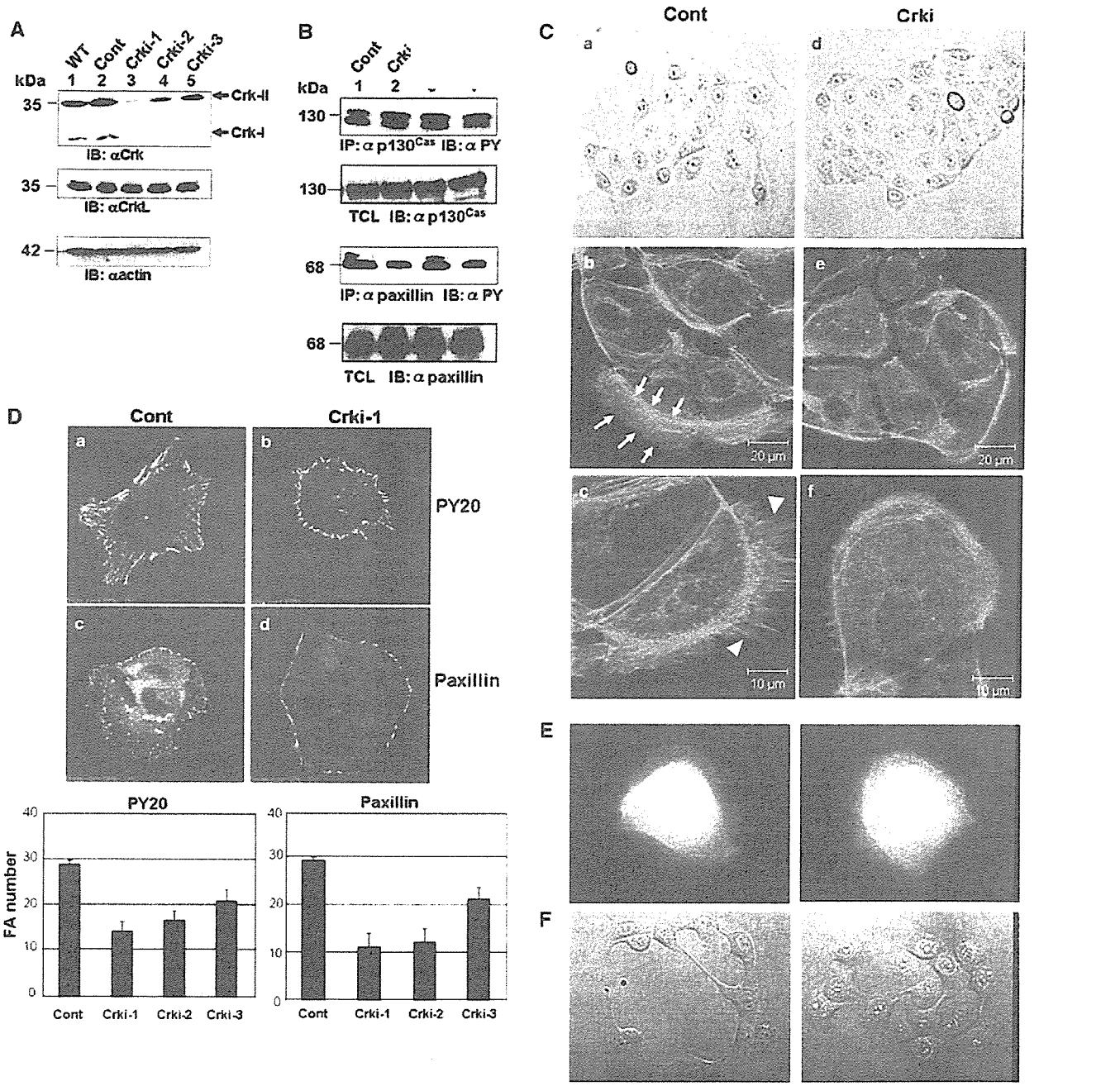

Figure 2 (**A**) Establishment of Crk knockdown MCAS cell lines. Total cell lysates of parental MCAS, control vector transfected cells or three Crk siRNA transfected cells (Crki-1, Crki-2 and Crki-3) were immunoblotted with anti-Crk, anti-CrkL or anti-actin Abs. The positions of Crk-I and Crk-II were indicated by arrow. (**B**) Tyrosine phosphorylation of p130^{Cas} and paxillin in Crk knockdown cells was analysed by immunoprecipitation and immunoblotting using total cell lysate. Total levels of p130^{Cas} and paxillin were also analysed by immunoblotting. (**C**) Morphology of parental (panels a–c) and Crk knockdown MCAS cells (panels d–f). Phase-contrast microscopical observation (panels a and d) and phalloidine staining (panels b, c, e and f). Arrow and arrowhead indicate lamellipodia and filopodia, respectively. (**D**) Immunofluorescence of control cells and Crk knockdown Crki-1 cells by antiphosphotyrosine (panels a and b) and antipaxillin (panels c and d) Abs. The numbers of focal adhesion were counted and described as bar graph with standard error. (**E**) GFP-actin transfected control (left panel) and Crk knockdown Crki-1 (right panel) cells. The results of time-lapse observation of these cells were available as Supplementary data. (**F**) Phase contrast microscopical observation of control (left panel) and Crk knockdown (right panel) cells 3 h after serum stimulation. (**G**) Transient transfection of both GFP-actin and RFP-Crk-I expression plasmids (panels a–c) or both GFP-actin and RFP (panels d–f) into Crk knockdown cells. RFP-Crk-I and GFP-actin were separately observed and displayed as upper (a and d) and middle (b and e) panels. Merged images were displayed at the bottom (c and f). The results of time-lapse observation of RFP-Crk-I expressed cells were available as Supplementary data. (**H**) Transient expression of myc-Crk-I and myc-Crk-II in Crk knockdown cells. Anti-myc Ab was used to detect overexpression of Crk (green). Phalloidine stain was performed to detect actin cytoskeleton (red). Yellow bar indicates 20 μm.